Photomechanical Processes and Effects in Ablation

Günther Paltauf*,† and Peter E. Dyer‡

Institute of Experimental Physics, Karl-Franzens-Universität Graz, Graz, Austria, and Department of Physics, University of Hull, Hull HU6 7RX, United Kingdom

Received June 5, 2002

Contents

I. Introduction

Photomechanical ablation is a process by which absorption of a laser pulse in a target creates mechanical stress that leads to material fracture and ejection. Steverding in an early publication[1] pointed out that ablation by fracture of a material into more or less large chunks is energetically orders of magnitude more efficient than the continuous removal of individual surface molecules by chemical reactions or by evaporation. This can be illustrated by an example of liquid ablation. To completely vaporize 1 mol of water at room temperature requires the vaporization enthalpy of 47 kJ. To break the same amount of water into droplets of 10 μm radius requires an energy for free surface generation equal to 0.76 J, a factor of $\sim 6 \times 10^4$ lower. Dingus et al.[2−4] brought photomechanical ablation into play as an interesting method to remove biological tissue. In tissue ablation it is not only important to achieve energetic efficiency but, in specific applications, it is also highly desirable to limit the extent of collateral thermal damage. Therefore, a process of "cold ablation", by which tissue can be removed without the necessity to vaporize it, attracted much attention.

There has been experimental evidence that under certain conditions photomechanical effects play a role in laser ablation. One observation is that the energy density threshold for tissue ablation with nanosecond laser pulses can be up to an order of magnitude lower than that needed for complete vaporization.[5] These low thresholds point strongly to mechanical effects being implicated in removal. Another observation is that ablation with these short laser pulses is accompanied by the radiation of strong acoustic waves into the ablated material. These acoustic transients can be a consequence of ablation, for example, due to the recoil momentum of vaporized and ejected material, in which case no waves are generated below the ablation threshold. If acoustic transients are generated below the ablation threshold by mechanisms other than recoil momentum, it is possible that their amplitude becomes so high that they actively cause material fracture and removal. Only in this case can one speak of photomechanical ablation. The question remains about the sources of sufficiently strong acoustic transients that are able to fracture a material and to eject the fragments. Early in the history of laser−material interactions Carome et al.[6] observed that irradiation of a liquid with a short laser pulse can cause acoustic waves, both compressive and tensile, with high amplitudes, even at laser pulse energies below the ablation threshold. These waves are due to localized heating and thermal expansion of the medium, leading to thermoelastic stress. The rapid release of this stress causes the emission of acoustic waves. In contrast to liquids, solids retain some of the stress and release it more slowly by

* Address correspondence to this author at Universitätsplatz 5, 8010 Graz, Austria (telephone +43 316 380 8556; fax +43 316 380 9816; e-mail guenther.paltauf@uni-graz.at).
† Karl-Franzens-Universität Graz.
‡ University of Hull.

10.1021/cr010436c CCC: $44.00
Published on Web 01/04/2003

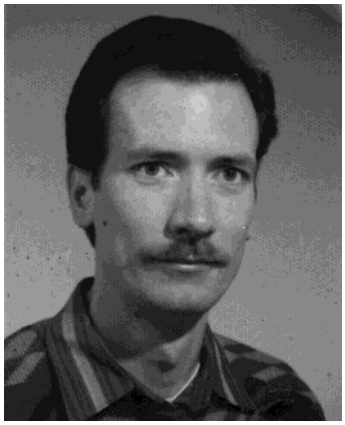

Günther Paltauf received his Ph.D. in experimental physics from Karl-Franzens-Universität Graz in 1993 with a thesis on photomechanical ablation mechanisms. Postdoctoral studies at the same university and further work at the Institute of Applied Physics at the University of Bern, Switzerland, and at the Oregon Medical Laser Center in Portland, OR, were devoted to photomechanical laser–material interactions and to methods to characterize materials, mostly biological tissue, by use of laser-optoacoustics. In 2001 he returned to the University of Graz, where he now holds the position of an associate professor in the Department of Experimental Physics. His current research interests include pulsed laser–material interactions and optoacoustic spectroscopy and imaging.

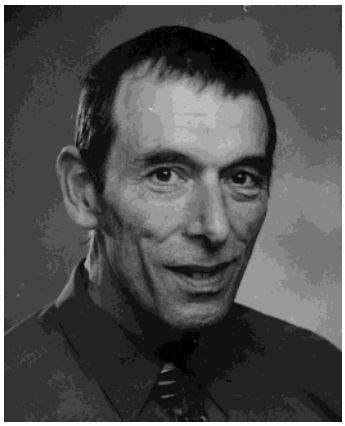

P. E. Dyer gained a B.Sc. and Ph.D. in applied physics from the University of Hull and has been involved in research on lasers, laser–materials interactions, and related optical physics since 1969. In the late 1970s his interest shifted from pulsed infrared CO_2 lasers to UV excimer lasers, and in 1982 he commenced work on UV laser ablation. Most recently his reserach effort has shifted to laser interactions in the VUV (vacuum ultraviolet) and to the application of infrared lasers for scleral buckling in ophthalmology. The research work has remained closely allied with industrial applications (e.g., micromachining, film deposition) and medical applications (e.g., MALDI analysis, photodynamic therapy, ophthalmology) and has benefited from collaborations with many organizations at the national and international levels. To date he has published 175 papers in the areas of laser, laser–materials interactions, laser ablation, and micromachining and on the application of lasers and optical physics in medicine. Professor Dyer gained a Personal Chair in Applied Physics at the University of Hull in 1989. From 1987 to 1997 he was Head of the Department of Applied Physics in the School of Engineering and Computing and from 1997 to 2001 Head of the Physics Department in the Faculty of Science.

thermal conduction into the surrounding material. The resulting transient and quasi-static thermoelastic stresses can cause weakening, fracture, and ejection of a material.

Fragmentation is also involved in other ablation mechanisms such as the “phase explosion” (explosive superheating) or in “confined boiling”, where the ejected material is in a mixed phase. The mechanical forces in this case are largely induced by the vaporized fraction.[7] These mechanisms are described in detail in the paper on tissue ablation by Vogel and Venugopalan in this issue and will not be reviewed here. There are also a number of cases of the removal of material through mechanical forces generated by laser-induced vaporization reported. Examples are the lift-off of a color coating layer,[8] metal film forward transfer,[9] and organic molecule implantation into various materials.[10] As the primary ablation force is not mechanical stress we exclude them from the scope of this review and, likewise, plasma-mediated shock waves as these involve a major phase change.

Here we will focus on fracture and ablation mechanisms that are caused by thermal expansion alone. For a better distinction between the different mechanisms, consider the energetic paths in pure photomechanical and phase change-induced ablation: In photomechanical ablation a fraction of the absorbed laser energy goes into elastic stress energy and a fraction thereof into plastic deformation of the target, generation of internal free surfaces (fracture by generation of cracks or voids), and kinetic energy of the ejected material. Negligible energy goes into a phase change, except some evaporation into voids and cracks. This is in contrast to fracture due to an explosive phase change when the driving force is the pressure in expanding vapor bubbles.

A perceived benefit of photomechanical ablation as opposed to phase change induced ablation is the low temperature in the remaining material, which is interesting for medical applications as it offers the potential to ablate tissue with minimal thermal side effects. However, because stress waves are involved, mechanical damage in surrounding tissue is possible. The penetration depth of these may be much larger than that of the light and thermal waves and, indeed, there are reports of collateral tissue damage attributed to acoustic waves.[11,12] Nevertheless, the very stress waves themselves may be put to good purpose as they carry information on the basic laser−material interaction phenomenon. For this purpose, various techniques with good spatial and temporal resolution have been developed and provide a useful way of monitoring the ablation process and the possible onset of fracture and material ejection.

Transient stress-induced material damage and ablation is known from shock wave research as “spallation”. In this damage mode a shock wave is created by either plate impact, explosive loading, or laser irradiation on one side of a target[13−15] (Figure 1). After crossing the target, the compressive wave arrives at the back surface. If there is an acoustical mismatch from high to low impedance, the compressive wave is partly (or fully at a free boundary) reflected and is converted into a tensile stress wave. At a certain depth below the surface the superposition of compressive and tensile stress waves gives a net tension. The dynamic tensile stress, if sufficiently high, leads to fracture and eventually the ejection of fragments of material. Because material fracture takes place after reflection at the back surface of a target, this damage mode is often termed “back

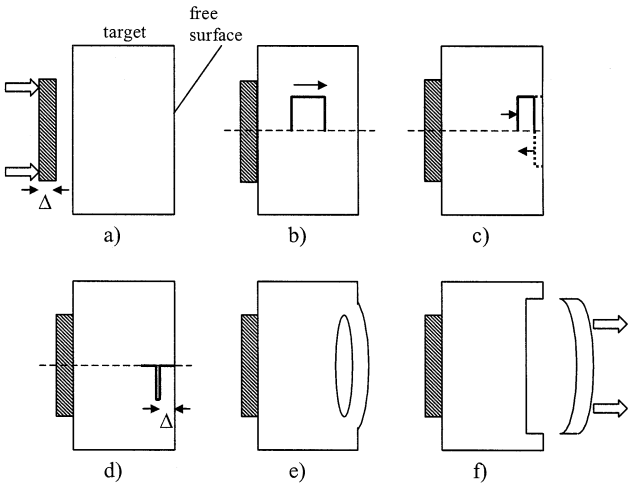

Figure 1. Back surface spallation: (a) impact of a flyer plate of thickness Δ at the front surface of the target launches a rectangular stress pulse (b); (c) reflection of the stress pulse at the free back surface; the incoming positive pulse is canceled by the reflected negative pulse in the vicinity of the surface; (d) first appearance of tensile stress at a depth corresponding to the flyer plate thickness; (e) if the stress exceeds the dynamic tensile strength, it will lead to fracture; (f) at a later stage the separated material breaks away and is ejected.

surface spallation". Ablation of the front side of a target after irradiation by a laser pulse follows a similar pattern (Figure 2): The laser pulse heats a

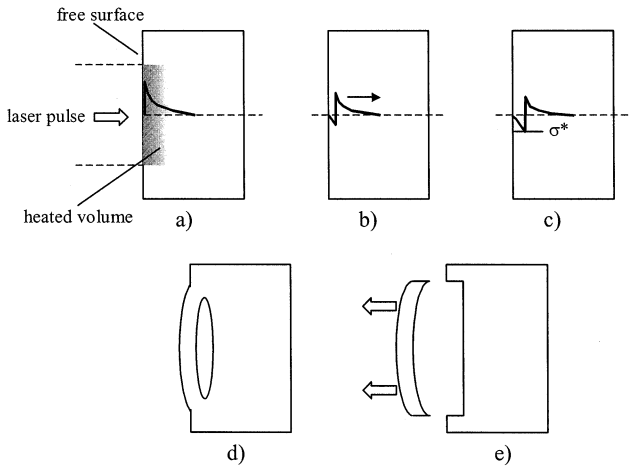

Figure 2. Front surface spallation or photospallation: (a) thermal expansion of the volume heated by a laser pulse causes mechanical stresses; (b) upon propagation from the free surface a tensile component develops with gradually increasing amplitude; (c) at some depth the tensile strength σ^* is exceeded and the material fractures; (d, e) detachment and ejection of material from the front surface.

surface layer and generates thermoelastic stress pulses in directions perpendicular to the surface, one propagating into the medium and one toward the free surface. Due to the acoustic mismatch the latter becomes negative and may cause material fracture at a certain depth, followed by the ejection of relatively cold fragments. Because it takes place at the front side of the target after the laser pulse impact the terms "front surface spallation" or "photospallation" have been used to describe this effect. There may be situations when both kinds of spallation are generated in a single experiment on both sides of a laser-irradiated target. If the target is a solid, the thermoelastic stress also contains quasi-static components, which compared to the transient acoustic stresses stay localized in and around the laser-irradiated volume and persist for much longer times. The damage induced by these stresses is therefore expected to evolve in a different way, in both its spatial and temporal behaviors.

Photomechanical laser ablation mechanisms have been discussed in several previous reviews,[16−18] but to our knowledge there has not been a review entirely devoted to these effects before. The present review will cover research that has been performed largely during the past 15 years, starting with the first systematic investigations of laser-induced acoustic waves during ablation of polymers.[19] In section II, we will outline the basic processes whereby transient and quasi-static thermoelastic stress are generated in laser-irradiated liquids and solids. These considerations will show where and when stresses develop in a target when a laser pulse heats it. In section III we will focus on the mechanisms of material damage and ablation that may arise from these stresses. This is followed by a discussion in section IV of the main evidence for photomechanical ablation by transient thermoelastic stress, both that arising from experimental studies and that from theoretical models which are being developed to describe the process. Section V discusses the various diagnostic applications of both the thermoelastic and ablative recoil-generated stress waves. The photomechanical ablation of layers as an important example where ablation by quasi-static thermoelastic stress has been demonstrated is the subject of section VI. Other areas in which the understanding of photomechanical effects could be beneficial such as in matrix-assisted laser desorption ionization (MALDI), laser surface cleaning, and laser marking will be briefly covered in sections VII−IX.

II. Photomechanical Stress Generation below the Ablation Threshold

A. Thermoelastic Effect

Here we describe stress generation mechanisms by impact of laser pulses in absorbing materials. We assume that the level of stress is insufficient to cause irreversible material damage. How laser-induced mechanical stress leads to fragmentation and ablation of materials will be described in section III. As discussed by Gusev and Karabutov,[20] among the various sources by which acoustic waves can be generated by impact of laser pulses, in absorbing media the thermoelastic effect is by far the most efficient below the ablation threshold. Other mechanisms such as photon momentum or electrostriction are either negligible or play a role only in transparent media.

It has to be mentioned that another efficient mechanism for stress wave generation that is almost independent of linear optical absorption is the formation of an optical breakdown plasma generated by focusing high-power laser pulses onto the surface or

into the bulk of a material. The high-temperature plasma in the interaction volume expands and emits a shock wave. This effect plays an increasing role in the precise ablation of materials. What is primarily utilized is the localized plasma, whereas the secondary mechanical effects are for the most part undesired, particularly in biological tissue. One way to reduce collateral mechanical effects is to reduce the pulse duration because optical breakdown with shorter pulses requires a higher laser irradiance but a lower pulse energy.[21] The mechanical damage range in turn scales with the total deposited energy. The mechanical effects of optical breakdown do play an important role in the interaction of short laser pulses with transparent media but do not lead to photomechanical ablation in the same way as the "cold" material ejection initiated by thermoelastic stress.

Thermoelastic stress is caused by the heating and thermal expansion of a material. If the heat generated by absorption of light stays confined in the irradiated volume during the laser pulse and cannot escape via heat conduction, a condition termed "thermal confinement" is obtained. The criterion is that the pulse duration has to be shorter than a characteristic thermal relaxation time t_{th}, given by

$$t_{th} = d^2/4\chi \tag{1}$$

where d is the smallest dimension of the heated volume (either the beam diameter or the optical penetration depth, whichever is smaller) and χ is the thermal diffusivity. Thermal confinement maximizes the temperature in the heated volume and is an important prerequisite to efficiently generate thermoelastic stress.

In a liquid, the overpressure p (in the following referred to as "pressure"), which is the difference between the actual pressure and the equilibrium pressure, depends on the relative volume change $\Delta V/V$ and the temperature change ΔT

$$p = -B(\Delta V/V) + B\beta\Delta T \tag{2}$$

where B is the bulk modulus and β the volume expansion coefficient.

For an isotropic solid, the equivalent equation is the stress−strain relationship[22]

$$\sigma_{ij} = \frac{3B}{1+\nu}[(1-2\nu)\epsilon_{ij} + \nu\epsilon_{kk}\delta_{ij}] - B\beta\Delta T\delta_{ij} \tag{3}$$

where σ_{ij} and ϵ_{ij} are the components of the stress and strain tensor, respectively, ν is the Poisson ratio, and δ the Kronecker symbol. Here we use the convention that compressive stress has a negative sign. The relative volume change is $\Delta V/V = \epsilon_{kk} = \epsilon_{11} + \epsilon_{22} + \epsilon_{33}$. From both relationships it follows that the maximum pressure or stress, $B\beta\Delta T$, is achieved if the heating takes place in a way that all displacements in the medium that would give rise to a volume change or any strain are zero. This condition is called stress or inertial confinement and is achieved if the heating pulse is much shorter than the characteristic time of acoustic relaxation, t_{ac}

$$t_{ac} = d/c_s \tag{4}$$

where c_s is the speed of sound. Stress and pressure lead to displacements in the medium. Using the equation of motion, one obtains for a liquid the scalar thermoelastic wave equation that is most conveniently given in terms of the velocity potential ϕ[20]

$$\nabla^2\phi - \frac{1}{c^2}\frac{\partial^2\phi}{\partial t^2} = \frac{\beta}{\rho C}S \tag{5}$$

where ρ is the density, C the specific heat capacity, and S the heat generated per unit time and volume. The relationships between pressure, particle velocity $\mathbf{v}$, and velocity potential are

$$\mathbf{v} = \text{grad}\ \phi \tag{6a}$$

and

$$p = -\rho(\partial\phi/\partial t) \tag{6b}$$

The corresponding wave equation for the displacement vector $\mathbf{u}$ in an isotropic solid is[22,23]

$$\rho\frac{\partial^2\mathbf{u}}{\partial t^2} - \frac{E}{2(1+\nu)}\nabla^2\mathbf{u} - \frac{E}{2(1+\nu)(1-2\nu)}\nabla(\nabla\mathbf{u}) = -B\beta\nabla(\Delta T) \tag{7}$$

where E is Young's modulus. A good description of the temporal evolution of thermoelastic stresses in a solid has been given by Albagli et al.,[23,24] according to which four regimes are distinguished:

(1) Heating phase under stress or inertial confinement. The maximum stress $B\beta\Delta T$ is achieved, which serves as the initial condition for the second regime.

(2) Transient regime, in which the forces caused by the thermal stress lead to displacements that propagate as longitudinal and transverse acoustic waves. The time scale for the emission of acoustic waves from the heated zone is t_{ac}.

(3) Quasi steady-state regime, in which the system reaches mechanical equilibrium and the net forces in any direction become zero. Due to the nonuniform temperature distribution that is caused by heating a confined volume within the medium, individual stress components are not zero. The existence of the third regime requires that $t_{ac} \ll t_{th}$, a condition that is always satisfied with the exception of extremely small values of d (in the sub-nanometer range). The quasi-static stresses strongly depend on the shape of the heated volume. For example, a rectangular laser beam profile generates much higher temperature gradients and stresses than a beam with a Gaussian radial profile.

(4) Thermal diffusion regime with a time scale of t_{th}, in which the excess heat diffuses out of the irradiated volume and the thermoelastic stresses decay to zero.

Because liquids can support neither shear waves nor any quasi-static stresses arising from thermal deformations, only regimes 1 and 2 occur in liquids and only longitudinal waves are generated.

The importance of transient and quasi-static stresses for the ablation process depends on the sign

and magnitude of the stresses, their orientation, and duration. Generally, materials are more likely to be damaged by tensile than compressive stress. Therefore, we will focus further discussion mainly on the occurrence of tensile stresses. Because in liquids only transient thermoelastic pressure can be generated, the condition of stress confinement has to be satisfied to maximize the pressure. As will be shown later, also in the case that stress confinement is not strictly obtained, significant pressure can be generated, but at higher temperatures and consequently with lower energetic efficiency. Near the irradiated liquid surface the propagating acoustic wave causes a displacement normal to the surface and a tension. The combination of both effects can ablate a liquid volume near the surface. In solids both transient and quasi-static stresses can contribute to ablation. The transient stress acts in a similar way as in liquids, but additional stress components such as radial stress right at the surface develop.[25] It is also possible to generate only the third and fourth regimes without transient stresses, as long as $t_p \ll t_{th}$. Quasi-static stresses mainly develop in regions where the temperature gradient is high.[24] A top-hat laser beam with sharp edges in the radial irradiance profile will therefore mainly cause strong stresses right at the rim of the laser beam. Alternatively, a difference of thermal expansion coefficients, for example, at the interface of a coating with a substrate that has a smaller thermal expansion coefficient, can cause stresses that initiate ablation of the coating.[26] Considering that dynamic fracture needs some incubation time (see section III.A) and that quasi-static thermoelastic stresses act orders of magnitude longer on the material than the transient stresses, even low amplitudes of quasi-static stress might play an important role in ablation.[24]

B. One-Dimensional Solution of the Thermoelastic Wave Equation in a Liquid

Many of the characteristics of transient stress-induced ablation can be studied using the case of one-dimensional thermoelastic waves generated at a free boundary. The properties of such waves were investigated experimentally and theoretically very early in the history of laser−material interactions.[6,27] Consider a uniformly absorbing target material with an absorption coefficient μ_a that is irradiated with a laser pulse with an energy Q. To generate a plane wave propagating perpendicular to the surface of the target, the radius of the laser beam should be much larger than the optical penetration depth $1/\mu_a$. Furthermore, the irradiance should be uniform over the entire area of the laser beam, giving a laser fluence $H_0 = Q/A$, where A is the size of the irradiated area. Some of the incident laser radiation is reflected at the surface and is therefore not absorbed in the target. For the sake of simplicity, we will assume in the following that H_0 is corrected for these reflection losses. Absorption of a laser pulse with $t_p \ll t_{ac}$ produces an initial pressure distribution $p_0(z)$

$$p_0(z) = B\beta\Delta T(z) = (B\beta/\rho C)\mu_a H_0 \exp(-\mu_a z) \quad (8)$$

It is useful to introduce a dimensionless quantity $\Gamma = B\beta/(\rho C)$, called the Grüneisen parameter, that relates the initial pressure to the absorbed volumetric energy density. Γ is 0.11 for water at room temperature and in the range of 0.1−0.2 for biological tissue. For polymers $\Gamma \approx 1$, and for glasses $\Gamma \approx 0.5$. The Grüneisen parameter may depend on temperature, which introduces some nonlinearity into the relationship between pressure and temperature. For water the temperature dependence of β causes an ~4-fold increase of Γ between room temperature and the boiling point.[28] The wave generated from the initial distribution consists of two parts with the same spatial profile as p_0, but half the amplitude, traveling in opposite z directions. The part propagating in the negative z direction is reflected at the surface with a reflection coefficient

$$R_{ac} = \frac{Z_2 - Z_1}{Z_2 + Z_1} \quad (9)$$

where Z_1 and Z_2 are the acoustic impedances ($Z = \rho c_s$) of the target and the surrounding medium, respectively. The wave at $z > 0$ is the superposition of three components

$$p(z,t) = p_1 + p_2 + p_3 \quad (10)$$

$$p_1 = 0.5 p_{0,max} \exp[-\mu_a(z - c_s t)] \quad z > c_s t$$

$$p_2 = 0.5 p_{0,max} \exp[-\mu_a(z + c_s t)] \quad z > 0$$

$$p_3 = 0.5 p_{0,max} R_{ac} \exp[-\mu_a(c_s t - z)] \quad c_s t > z > 0$$

$$p_{0,max} = \mu_a \Gamma H_0$$

Figure 3a shows the temporal evolution of a wave in the case that a free surface is irradiated, where $Z_2 \approx 0$ and $R_{ac} = -1$. At each point below the surface the pressure consists of a compression followed by a rarefaction, the latter having an amplitude that rises with depth (dashed line in Figure 3a). At a depth of $1/\mu_a$ the tensile stress amplitude reaches 43% of the initial compressive pressure amplitude. In the context of ablation not only the tensile stress but also the heating contributes to a weakening of the material, causing melting or some other thermal decomposition (e.g., thermal denaturation of biological tissue). Therefore, it is of interest to know the product of tensile stress amplitude and temperature rise, which is plotted in Figure 3b. A maximum of this quantity occurs near a depth of $0.5/\mu_a$. During reflection of p_2 at the free surface, whereby it is converted into p_3, the liquid is set into motion toward the free surface with a maximum velocity of p_0/Z_1. A laser pulse that heats water from room temperature to the boiling point creates $p_0 = 1$ kbar, giving with $Z_1 = 1.5 \times 10^6$ kg m^{-2} s^{-1} a flow velocity of 67 m/s.

The influence of a finite laser pulse duration can be taken into account by calculating the convolution of the temporal pressure distribution at a certain position with the temporal profile of the heating pulse

$$p(z,t) = g(t) \otimes p_\delta(z,t) \quad (11)$$

Here, $g(t)$ is the temporal pulse profile, the sign $\otimes$

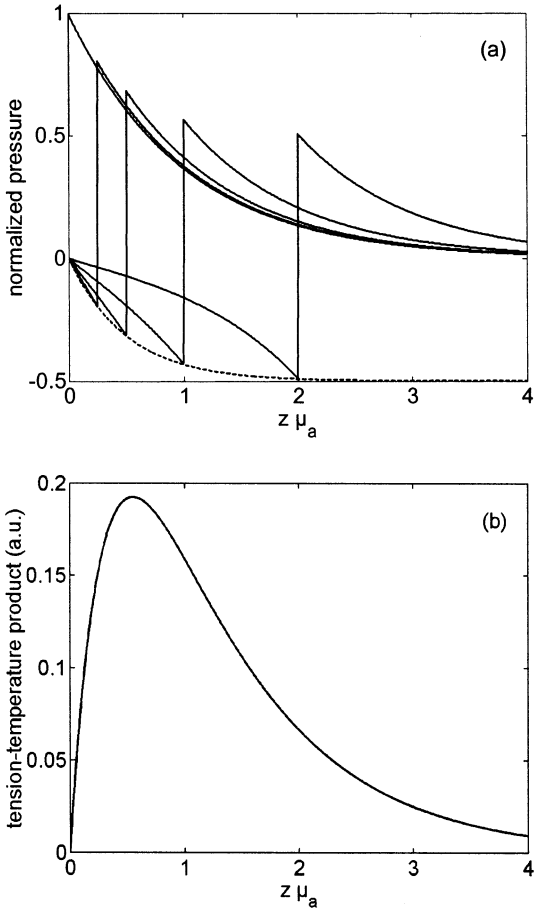

Figure 3. One-dimensional thermoelastic stress wave generated at a free surface, calculated for instantaneous heating (infinitesimal laser pulse duration): (a) normalized pressure plotted at 0, 0.25, 0.5, 1, and 2 times the acoustic relaxation time as a function of relative depth in units of the optical penetration depth $1/\mu_a$ (the dashed line is the envelope of the tension amplitude); (b) product of tensile stress amplitude and temperature rise as a function of relative depth.

denotes convolution, and p_δ is the solution derived above for an infinitesimally short (delta function) pulse. If the pulse duration becomes comparable with the acoustic relaxation time, that is, if the stress confinement condition ceases to be valid, smearing with the function $g(t)$ will diminish the amplitude of the acoustic wave. For a rectangular temporal laser pulse profile the ratio, A_{ac}, of the thermoelastic stress wave amplitude for a finite pulse duration to the amplitude for instantaneous heating can be described by an analytical expression[2]

$$A_{ac} = [1 - \exp(-\tau)]/\tau \qquad (12)$$

where $\tau = t_{p/tac}$. Figure 4 shows A_{ac} together with the corresponding factor for a laser pulse with a Gaussian temporal pulse profile with a full width at half-maximum of t_p. The latter was calculated by use of the convolution in eq 11. It can be seen that the attenuation is stronger for a Gaussian than for a rectangular pulse. A laser pulse with $\tau \gg 1$ produces a pressure profile that is determined by the temporal shape of $g(t)$ rather than by the distribution of absorbed energy. This offers the possibility to generate acoustic pulses with arbitrary shape as has been demonstrated for free electron lasers.[29]

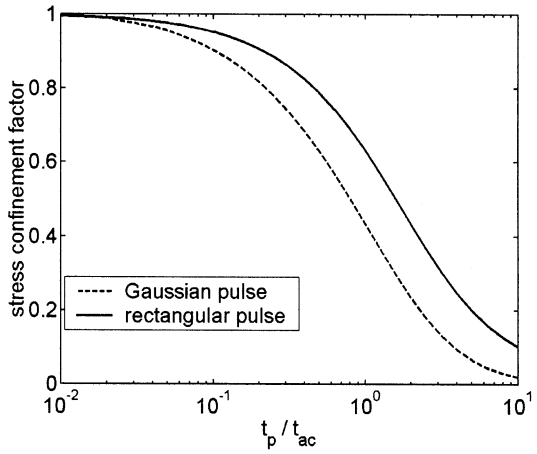

Figure 4. Stress confinement factor A_{ac}, defined as the amplitude of the thermoelastic stress wave for a pulse duration t_p divided by the amplitude for instantaneous heating, as a function of the ratio t_p/t_{ac}. Two curves for different temporal pulse profiles are shown.

A more complete treatment of optoacoustic generation in a liquid is given by Gusev and Karabutov.[20] The spectral method used there is based on transfer functions to describe the influence of the finite pulse duration and the initial temperature distribution and is also able to include effects of acoustic nonlinearity (due to the finite pressure amplitude), sound dissipation, and acoustic diffraction. Except for diffraction effects in the near field of the interaction zone, which will be treated below, the other two effects play a minor role in the ablation because they become significant only after the acoustic wave has propagated some finite distance into a medium.

If the stress confinement condition is satisfied in an experiment, then the time-resolved measurement of a one-dimensional stress transient at a depth $>1/\mu_a$ directly yields $p_1(t)$, which exactly follows the depth distribution of absorbed energy. This is a very useful method for measuring the optical properties of an optically thick medium.[30] In clear media without optical scattering, analysis of the temporal profile of pressure signals gives the absorption coefficient as a function of depth.[31,32]

C. Three-Dimensional Solutions of the Thermoelastic Wave Equation in a Liquid

If the finite size of the laser beam is taken into account, the wave generation problem becomes three-dimensional. The heated volume after absorption of a circularly symmetric laser beam has a disklike shape. Thermoelastic wave generation from such a source has been treated by including acoustic diffraction effects.[20,33] Another powerful method uses a retarded Green's function that, in principle, makes it possible to calculate thermoelastic waves from arbitrary, three-dimensional sources.[34,35] The only limitation is that this method assumes a homogeneous medium without impedance mismatched boundaries. However, this limitation can be overcome by the use of image sources.[36] The Green's function method gives the following solution of eq 5 for an

infinitesimally short laser pulse using $S(\mathbf{r},t) = W(\mathbf{r})\delta(t)$, where $\delta(t)$ is the Dirac delta function and W the volumetric energy density.

$$\phi(\mathbf{r},t) = -\frac{t}{4\pi\rho}\frac{\beta c^2}{C}\iint_{|\mathbf{r}-\mathbf{r}'|=c_s t} W(\mathbf{r}')d\Omega = -\frac{t}{4\pi\rho}\iint_{|\mathbf{r}-\mathbf{r}'|=c_s t} p_0(\mathbf{r}')d\Omega \quad (13)$$

$\mathbf{r}$ and $\mathbf{r}'$ are the observation point and a point in the source volume, respectively, and $d\Omega$ is the solid angle element. The integration is performed over the surface of a sphere with radius $c_s t$ around point $\mathbf{r}$. Figure 5 shows temporal pressure distributions at a

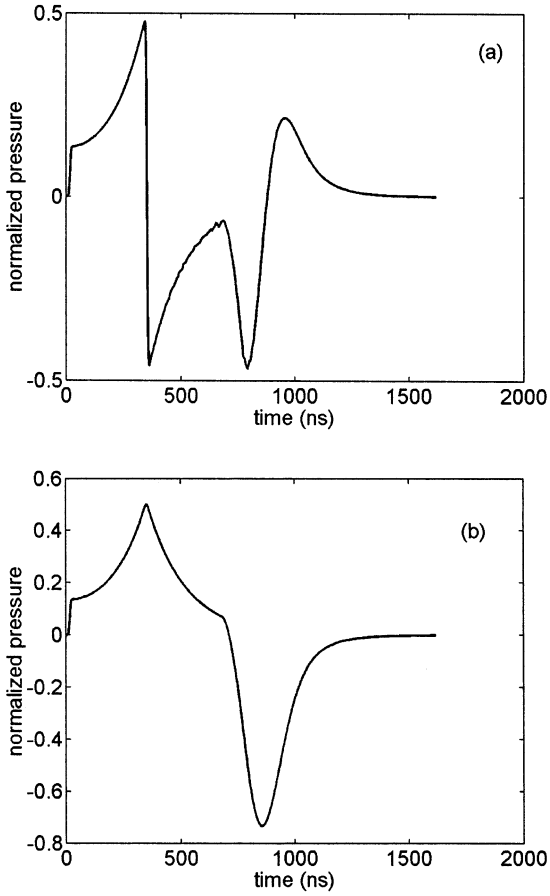

Figure 5. Pressure as a function of time calculated for a laser pulse duration of 10 ns at a depth of 500 μm = $2/\mu_a$ with $\mu_a = 4000\ m^{-1}$: calculation for (a) free surface and (b) rigid surface. The laser beam has a trapezoidal Gaussian radial profile with a radius of 1.2 mm.

point on the symmetry axis of the incident laser beam, both for a free and for a rigid surface. Rigid means that the surface of the absorbing liquid is covered by a medium with much higher acoustic impedance such as glass. In the case of the free surface, a point in the liquid first sees the plane wave arriving from the surface and then an inverted and smaller wave coming from the lateral boundary of the heated volume. Due to the symmetry of the latter, the radial wave has the biggest amplitude around the beam axis. In the signal from the rigid surface, reflection at the high-impedance interface results in a positive pressure component p_3 in eq 10. Therefore, the plane wave generated at the rigid surface is unipolar, but the radial wave is purely tensile.

The one-dimensional solution is sufficient to predict the ablative effect of transient stresses in cases when most of the heated volume first experiences the reflected negative pressure pulse from the surface and then the negative component of the radial wave. This is always valid for large laser beam radii compared to the optical penetration depth. If the beam diameter becomes comparable with the penetration depth, significant tensile stresses can develop in parts of the heated volume due to the radial wave component and can support the liquid fracture. In the case of a rigid boundary, the radial wave alone causes tensile stress. Liquid fracture is in this case manifested by cavitation around the laser beam axis.[37]

Sometimes a medium is optically heterogeneous and the absorption is concentrated in small zones or particles. An analysis of the cases where stress is not confined within the absorbing zones (i.e., $t_p > R_{ab}/c_s$, where R_{ab} is the radius of the absorber) and where different degrees of acoustic and thermal relaxation between individual zones are achieved has been carried out by Karabutov et al.[31] Depending on the size and density of such absorbers, the acoustic field in its general form is a superposition of a contribution depending on an average absorption coefficient and of acoustic pulses from individual absorbers. The time-dependent pressure pulse from one individual absorber is proportional to the time derivative of the laser pulse intensity but does not depend on the shape of the absorber. For larger absorbing zones in which both heat and stress stay confined during the laser pulse (i.e., $t_p < R_{ab}/c_s$), the general treatment for cylindrical and spherical geometry shows that the acoustic pulses depend on the shape of the absorber and that always more or less strong tensile stresses are generated.[35,38] The tensile stresses are implicated in the internal fracture of absorbing inclusions in tissue.[39−42] Solutions for the transient thermoelastic stresses inside optically thin spheres have been found by Sun and Gerstman.[40] The Green's function solution has been useful for obtaining solutions in spherical and cylindrical absorbers with arbitrary absorption, also including the optically thick case.[41] Figure 6 shows the time-dependent pressure signals in the center of an optically thin sphere for different laser pulse durations. The peak tensile stress depends strongly on the ratio t_p/t_{ac}.

D. Solutions for Solids

Three-dimensional solutions for the transient and quasi-static regime in solids have been given by Albagli et al. and Itzkan et al.[23−25] The transient solution was obtained by integrating eq 7 on a spatially uniform grid using the Adams−Bashforth time-stepping method. As well as the bipolar compressive−tensile stress pulse propagating in a direction perpendicular to the free surface in a similar manner as in a liquid, also transient radial stress is generated right at the surface (Figure 7a). The authors argue that the bipolar plane wave from the

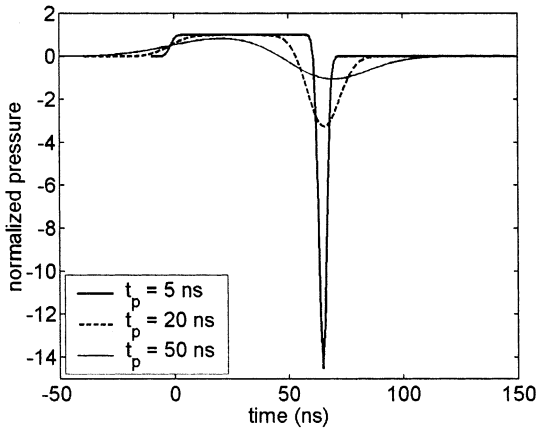

Figure 6. Pressure as a function of time in the center of an optically thin sphere with a radius of 100 μm, calculated for different pulse durations t_p. The tensile amplitude strongly depends on the laser pulse duration, although stress confinement conditions are satisfied for all pulse durations.

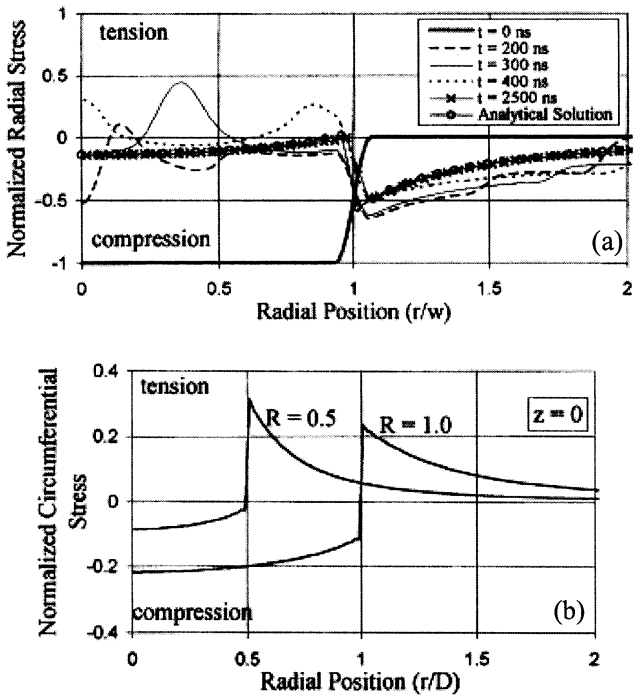

Figure 7. (a) Transient radial and (b) quasi-static circumferential stress normalized to the maximum initial compressive stress. In the calculation the thermoelastic stress generation in a material with $\rho = 1200$ kg/m^3, a longitudinal sound speed of $c_s = 2850$ m/s, and $\nu = 0.25$ by a short ($t_p \approx 10$ ns) laser pulse is simulated. r is the radial position, w the beam radius, D the optical penetration depth, and R the aspect ratio, given as $R = w/D$. Reprinted with permission from ref 23. Copyright 1995 National Academy of Sciences, U.S.A.

surface attains sufficient tensile amplitude to initiate failure only at a depth that is a considerable fraction of the laser penetration depth $1/\mu_a$, which cannot explain the very shallow ablation depths that are sometimes observed. It therefore seems likely that the radial stress components at the surface play an important role in ablation. Another result of the three-dimensional solution is the time dependence of the surface displacement. Comparing this result with measurements, it is possible to obtain material properties such as the transverse and longitudinal speeds of sound, the Poisson ratio, the optical penetration depth, and the Grueneisen coefficient.[23,43] An analytical solution of eq 7 for the steady-state displacements and stresses revealed that considerable radial, circumferential, and shear stresses persist during the quasi-steady-state regime (Figure 7b).

E. Energetic Considerations

An important question is the energetic efficiency of thermoelastic stress generation. A compression from ambient pressure to p_0 requires a work per unit volume, q, given by

$$q = (1/2B){p_0}^2 \tag{14}$$

For the case of stress confinement, integrating over the exponential distribution of p_0 defined in eq 8 gives the total potential energy, Q_c, stored in the compression of the heated volume

$$Q_c = (A/4B)\Gamma^2\mu_a{H_0}^2 \tag{15}$$

where A is the cross-sectional area of the laser beam. In a liquid, this energy is coupled into the acoustic wave that is radiated from the heated volume. Division by the laser pulse energy $Q = AH_0$ yields an energetic efficiency

$$(Q_c/Q) = (1/4B)\Gamma^2\mu_a H_0 \tag{16}$$

This gives quite low values; for example, the conversion efficiency of laser to stress energy is only 1.3×10^{-6} for a thermoelastic pressure amplitude $\Gamma\mu_a H_0$ of 1 bar generated in water. The efficiency is lower if stress is radiated during the pulse by an approximate factor of t_{ac}/t_p, a result that follows from including the attenuation factor A_{ac} (eq 12) in p_0 and taking into account that the duration of the acoustic wave is of the order of t_p.

There is a difference between the efficiency of acoustic wave generation in a liquid and in a solid because the solid can retain quasi-static thermoelastic strain energy after radiating the wave. When there is stress confinement and the laser spot size is much larger than $1/\mu_a$ so that the geometry is purely one-dimensional, the fraction, f_r, of Q_c radiated is

$$f_r = \frac{1+\nu}{3(1-\nu)} \tag{17}$$

and the fraction remaining as quasi-static thermoelastic strain energy, f_{qs}, is

$$f_{qs} = \frac{2(1-2\nu)}{3(1-\nu)} \tag{18}$$

For example, with $\nu = 0.2$, $f_r = f_{qs} = 50\%$. The liquidlike case with $\nu = 0.5$ gives $f_r = 100\%$ and $f_{qs} = 0$ as expected.

This picture will alter when the one-dimensional condition is no longer valid; that is, the laser spot size becomes comparable with $1/\mu_a$ as boundary effects become increasingly important.

The stresses are more complicated under these conditions[24] and will result in different expressions for the energetic efficiencies.

III. Fracture and Ablation Mechanisms

A. General Material Fracture

In this section we review the basic mechanisms of dynamic material fracture due to mechanical stress. This problem has been investigated in shock wave research over a long period, and here we restrict our considerations to the basic mechanistic aspects. Shock wave experiments use mainly the back surface spallation geometry. It has to be noted that although in principle front and back surface spallations are similar, the former takes place in a part of the target that is heated by the incident laser radiation. This heating might in some way weaken the material and reduce its strength. Molecular dynamics simulation models that take into account this complication are discussed below in Section III.C.

A simple model for fracture due to stress transients assumes that the material has a certain tensile strength and that fracture takes place at the time and location where the amplitude of the stress exceeds this threshold. For one-dimensional propagation of the stress transient (in either front or back surface spallation) this gives a defined depth below the surface where the material is separated and new free surfaces are generated. The residual stress that propagates toward this surface will again result in tensile stress that may reach the failure strength and generate a new spall plane and so on.[2] Following this simplified model, several layers are ejected. In front surface spallation the total ablation depth is comparable with the optical penetration depth. Using the solution of the one-dimensional thermoelastic wave equation (eq 10) with $R_{ac} = -1$, the first spall plane should be generated at a depth z^*, where the sum of the pressure components p_2 and p_3 first reaches the tensile strength, p^*

$$z^* = -\frac{1}{2\mu_a}\ln\left(\frac{2p^*}{\mu_a \Gamma H_0} + 1\right) \qquad (19)$$

This model oversimplifies the material failure, mostly because it does not take into account that the fracture process is time-dependent. A realistic spallation model should also distinguish between brittle and ductile fracture, depending on the nature of the material and also on the strain rate.[13,44] Fracture evolves from nuclei that grow under the action of the tensile stress and eventually coalesce, forming the spall layer. In ductile materials the voids are nearly spherical and their growth is accompanied by plastic deformation. Brittle fracture is governed by dynamic crack propagation without large-scale plastic deformation.[45] In spallation there are various degrees of material failure that are achieved with increasing stress amplitude or with decreasing material strength.[3] Incipient spallation is said to occur if the threshold for the void or crack formation is just exceeded but no coalescence takes place. The next degree is coalescence of voids or cracks and the formation of a spall layer, which is not necessarily ejected if it does not have sufficient momentum to break loose at the periphery. The highest degree finally is achieved if the material breaks loose at the periphery and is ejected. These degrees have been observed in rear surface spallation experiments in metals.[14] Due to the similarity of the two processes, they are also expected to happen in front surface spallation.

The time dependence of spallation is due to the dynamics of voids and cracks that grow under the action of tensile stress. In solids, growth has been found to linearly depend on current void size and pressure level, giving rise to an exponential growth with time as long as the voids are small.[46] As a result, the final stage of damage depends on the complete stress history and it is not possible to give a certain tensile stress at which fracture occurs. To accurately know the stress−time dependence under various experimental conditions is therefore an important prerequisite to predict the outcome of dynamic fracture. Much of the work to investigate dynamic material fracture has been done in plate impact experiments, where a flyer plate impacts a target with defined speed generating a rectangular compression pulse. From the impact velocity and the thickness of the flyer plate the duration and amplitude of this pulse and consequently the time history of the tensile stress after its reflection at the rear surface of the target are well-defined. To generate different stress histories in a single experiment, tapered flyer plates have been used giving different durations of the tensile pulse across a sample and accordingly different degrees of material damage.[46] In experiments using explosive loading or a laser-induced plasma at the front surface of the target the resulting shock waves have nearly triangular shape.[47,48] Also in these experiments the tensile stress versus time near the back surface of the target is relatively well-defined. In laser-induced front surface spallation initiated by transient stress in the regime of stress confinement, the temporal stress history is given by the solution of the thermoelastic wave equation. The duration of the stress wave is determined by the acoustic relaxation time defined in eq 4. For a small optical penetration depth compared to the laser beam radius the size of the heated volume is $d = 1/\mu_a$, giving $t_{ac} = 1/(\mu_a c_s)$. For a given material it therefore depends only on the absorption coefficient, which can be changed by varying the laser wavelength.

For a known stress history the cumulative damage concept of Tuler and Butcher[47] can be used to predict the time dependence of spallation. According to this empirical model, fracture occurs in a particular plane if a damage integral exceeds a critical value K. The damage criterion is given by

$$\int_0^{t_f} (\sigma - \sigma_0)^\lambda \, dt = K \qquad (20)$$

where t_f is the fracture time, σ_0 is a threshold value at which no fracture occurs even at a very long observation time, λ and K are constants, and $\sigma = \sigma(z,t)$ is the stress history at the spall plane. This

relationship gave values for spall layer thickness in aluminum in satisfactory agreement with experiments, using $\lambda = 2$. With $\lambda = 1$, the damage integral simply becomes a criterion for the impulse per unit area.

The energetic conditions necessary to achieve spallation were used by Grady to predict values for spall stress and time.[13] In this analysis the material is assumed to be exposed to a constant strain rate $\dot{\epsilon} = -\dot{\rho}/\rho$, giving rise to a linearly increasing tension

$$\sigma = B\dot{\epsilon}t \tag{21}$$

Spallation occurs if the elastic energy per volume, $\sigma^2/2B$, reaches a value equal to the energy U_f that is necessary to produce either coalescence of cracks for brittle or voids for ductile materials, that is

$$\sigma^2/2B = U_f \tag{22}$$

The fracture energy for brittle materials depends on the size of fragments, s, and a material property K_c, called the critical stress intensity factor or fracture toughness

$$U_f = 3K_c^2/\rho c_s s \tag{23}$$

The spall strength has then been shown[13] to scale with the cube root of the strain rate

$$\sigma^* = (3\rho c_s K_c^2 \dot{\epsilon})^{1/3} \tag{24}$$

In ductile materials the surface energy of the newly created voids is neglected compared to the plastic dissipation, and therefore there is no fragment size dependence of the fracture energy

$$U_f = Y\epsilon_c \tag{25}$$

where Y is the flow stress and ϵ_c is a critical strain where coalescence of voids takes place. A criterion for coalescence is that the void diameter approaches the void spacing, giving 0.15 as an appropriate value for ϵ_c. The fracture stress in this analysis becomes independent of strain rate

$$\sigma^* = (3\rho c_s^2 Y\epsilon_c)^{1/2} \tag{26}$$

From these energetic considerations also relationships for the time at which spallation occurs and the fragment sizes were obtained.[13] The strain rate dependence of the brittle fracture strength implies that there should exist a critical strain rate at which a transition from brittle to ductile takes place. Indeed, ductile fracture in aluminum that usually fails through brittle fracture has been observed at ultrahigh strain rate loading.[44]

The two models outlined above are slightly different, although eq 20 with $\lambda = 2$ also becomes a criterion for the energy. However, even if the energy is constant (i.e., σ is constant), Tuler and Butcher's model gives a finite waiting time that can be attributed to the time necessary for the voids or cracks to grow and coalesce. Grady's analysis, on the other hand, assumes instantaneous fracture once the necessary energy has been reached. The only way in which he includes growth dynamics is via a "horizon condition", stating that at a given time t the fragment size cannot be larger than $2c_s t$. This constraint on the fragment size at fracture in turn results in a condition for the brittle fracture energy, because generation of smaller fragments needs more energy for the generation of free surfaces. The energetic analysis by Grady also assumes that the stress and the elastic energy rise until the fracture criterion is reached. In the damage model of Tuler and Butcher, on the other hand, no assumption about the exact stress history is made.

In solids the quasi-static thermoelastic stress lasts for a time that is approximately given by t_{th}, whereas the transient stress decays over a time interval equal to t_{ac}, which is usually orders of magnitude shorter. According to the cumulative damage models outlined above the longer time over which quasi-static stress remains should result in a strong reduction of the fracture stress. In Tuler and Butcher's model the spall strength should approach σ_0, which may be the static fracture stress or, in ductile materials, the dynamic yield stress. As concluded by Albagli et al., this makes it likely that the quasi-static stresses, although smaller than the transient stresses, produce damage and assist ablation.[24]

B. Liquid Fracture

In a liquid, the fracture process is very similar to that of a ductile solid. Exceptions are highly viscous liquids with glass as the upper limit, where fracture is brittle.[13] The generation and growth of voids in a liquid under tension is usually called cavitation, and the conditions at which cavitation is generated due to stress characterize the tensile strength of a liquid. Various theories exist for the tensile strength of liquids:[49] The first theory states that fracture occurs if the external (negative) pressure exceeds the internal pressure caused by intermolecular forces. In the case of water this gives a value in the range of 10 kbar, much too high compared to experimental values that lie around 300 bar. The second theory is based on macroscopic thermodynamic arguments, requiring that the liquid should reach a state at which its van der Waals isotherm has a minimum, that is, where $dp/dV = 0$. This is the maximum superheated state above which the liquid becomes unstable. Between this state and the saturation state the liquid is metastable and cavitation may occur if there is a nucleation center, such as a pre-existing gas bubble or a partially wetted impurity. The superheat limit can also be reached at positive pressure, for instance, by isothermal decompression from saturation pressure or by isobaric heating. At atmospheric pressure this is found to occur at $\sim 0.84T_c$, where T_c is the critical temperature, based on the classical van der Waals equation of state (which is accurate for gases but not as good for liquids; more accurate theories for liquids give slightly different values[49]). The tensile strength should therefore rather be defined as the difference between the ambient pressure at the minimum of the isotherm and the saturation pressure at the given temperature.[49] The third way to predict the tensile strength of a liquid uses nucleation

theory and can be regarded as the microscopic explanation of the thermodynamic theory.[49] According to the nucleation theory used by Fisher,[50] at a given ambient pressure there exists a critical size of bubbles that corresponds to an energy barrier. Bubbles larger than the critical size are unstable and grow spontaneously, whereas smaller bubbles tend to disappear. At a given liquid temperature there exists a negative pressure at which the nucleation rate, that is, the number of bubbles created per unit time and mole, starts to rise sharply. Cavitation is said to occur if the nucleation rate reaches a threshold value, which in turn gives a value for the tensile strength. The rise of nucleation rate with negative pressure is so sharp that the calculated tensile strength hardly depends on the threshold nucleation rate. In the theory of Kwak and Panton, instead of the energetics of voids the conditions for the formation of clusters of higher energy molecules are used to derive a criterion for the tensile strength.[49] They arrive at a lower threshold for cavitation of water than Fisher.

Apart from the homogeneous nucleation that occurs only in a highly purified liquid, cavitation can also be initiated by heterogeneous nucleation. If there are pre-existing nucleation sites with a size R_h, in a first approximation the tensile strength of the liquid is reduced to $2\sigma_s/R_h$, where σ_s is the surface tension. In this approximation it is assumed that the pressure has to overcome the overpressure caused by the surface tension in a spherical bubble with size R_h. A more accurate equilibrium calculation gives the Blake threshold[51]

$$p_b = p_0 + 0.77(\sigma_s/R_h) \tag{27}$$

where p_0 is the ambient liquid pressure and p_b the negative acoustic pressure at which a bubble of initial size R_h will grow. It is assumed that $2\sigma/R_h \gg p_0$. The above definition of threshold pressure is strictly only valid for quasi-static conditions. For cavitation generated by the short thermoelastic stress transients inertial effects are likely to hamper cavity generation and the Blake threshold has to be taken as a lower limit. Most of the relationships that have been derived for nonstatic conditions take into account the relationship of the bubble resonance frequency with the frequency of a continuously oscillating sound field and are not directly applicable to the case of single stress transients.[51]

The threshold conditions for fracture and ablation of a liquid are determined not only by the initiation of cavitation but also by the growth and coalescence of the cavities and the subsequent ejection of liquid. As in solids, these dynamic effects are responsible for a time dependence of the fracture process, and a simple tensile strength is insufficient to describe the conditions for the initiation of liquid ablation. The dynamics of an ensemble of cavities in a liquid is very complex and requires complicated hydrodynamic modeling. In an early stage of cavitation, however, the cavities can be regarded as independent, and a general equation for the radial motion of an expanding or collapsing gas bubble in a liquid can be used to describe their dynamics. Such an equation has the form[51]

$$R\ddot{R} + \frac{3}{2}\dot{R}^2 = \frac{1}{\rho}(p_L - p_\infty) \tag{28}$$

where p_L is the time-dependent pressure in the liquid at the bubble wall, p_∞ is the pressure in the liquid at infinite distance from the bubble, and R is the bubble radius. Various modifications exist for this fundamental equation to include the effect of gas filling in the bubble, viscous damping of the bubble motion, and the compressibility of the liquid. An overview of the various models for cavitation bubble dynamics can be found in the book by Young and in references cited therein.[51]

The dynamics of a single cavitation bubble generated by a tensile stress pulse were modeled by Wentzell and Lastman to describe liquid fracture phenomena after reflection of a shock wave at a free surface.[52] This experimental condition is very similar to the various standard spallation experiments used to study dynamic fracture of solids. To model cavitation dynamics under these conditions, a negative pressure pulse given by some function $p(t)$ that drives the motion of the bubble was added to p_∞ in eq 28. Using this simplified model of liquid fracture, some experimental observations could be explained such as the changes in amplitude and temporal behavior of the reflected tensile pulse due to cavitation.[53] The pressure pulse driving the bubble motion was assumed to be an exponentially decaying function with finite rise time. In the presence of cavitation the peak of this wave was limited to approximately the cavitation threshold of the liquid and its temporal length was reduced to a short spike. Additionally, a prolonged tensile tail with a duration comparable to calculated bubble lifetimes was found in experiments. As will be shown later, these changes of the tensile pulse are also an indicator for photomechanically induced cavitation.

A similar model for front surface spallation of a liquid by transient thermoelastic stress based on heterogeneous nucleation has been described by Strauss et al.[54,55] This is a more accurate description of the cavitation process as it is a self-consistent model that at each time takes into account the pressure change due to the opening cavities. A one-dimensional hydrodynamic code was coupled to an ensemble of impurities with an exponential size distribution that acted as nucleation sites. The distribution of bubble sizes used in this simulation was given by

$$n = n_0/R_0 \exp(-R/R_0) \tag{29}$$

where $n\,\mathrm{d}R$ is the number of nuclei per unit volume with radius R in the range $\mathrm{d}R$, n_0 is the total number of nuclei per unit volume, and R_0 is a size parameter of the distribution. The use of a size distribution is another improvement over the simple model described above that assumed a certain initial size of a single nucleus. In the self-consistent model, voids are nucleated and grow under the action of tensile stress. The growing bubbles influence the pressure and density of the liquid, which in turn affects the further growth of the bubbles. The modification of the temporal pressure profile at a fixed depth below the

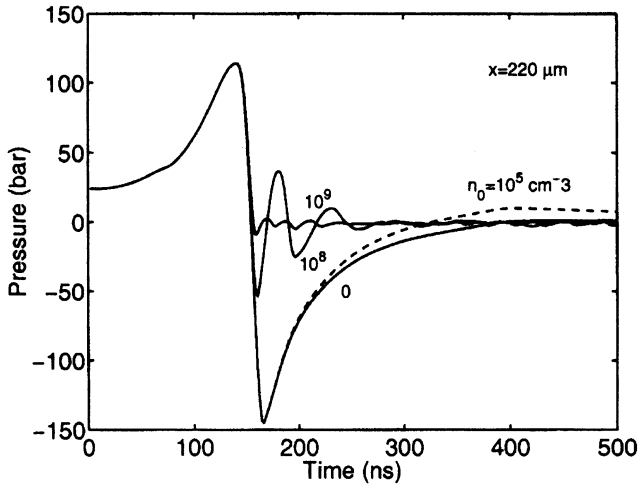

Figure 8. Calculated pressure versus time curves at a distance of 220 μm from the free surface of an absorbing liquid with $\mu_a = 10^4$ m^{-1} after irradiation of the surface with a laser pulse having a duration $t_p \approx 10$ ns that satisfies $t_p \ll t_{ac}$ and a fluence of 1.53×10^4 J m^{-2}. The liquid is at an ambient pressure of 1 bar. Calculations for different impurity concentrations, $n_0 = 0$, 10^5, 10^8, and 10^9 cm^{-3}, show that with increasing density of nucleation sites the influence of cavitation on the stress waves becomes stronger. Reprinted with permission from ref 55. Copyright 2002 American Institute of Physics.

surface for different values of n_0 is shown in Figure 8. At a given fluence, and hence pressure amplitude, the reduction of tensile stress due to bubble growth becomes stronger with increasing density of nucleation sites. This screening effect shifts the distribution of cavitation bubbles toward the liquid surface and causes fewer bubbles to be generated deeper in the liquid (Figure 9). Maximums of the distributions

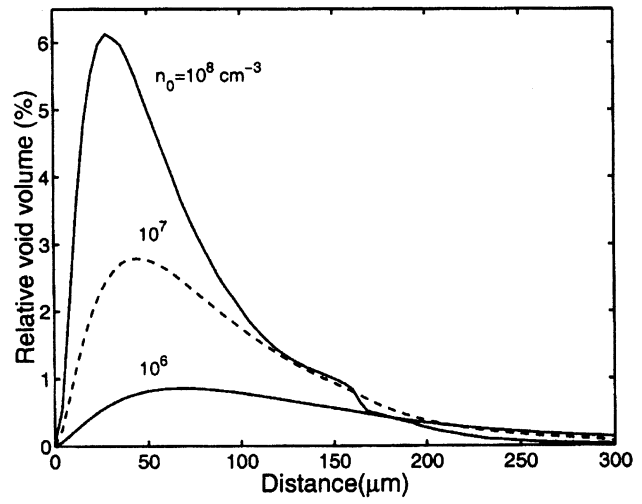

Figure 9. Calculated relative void volume distribution of cavitation bubbles for different nuclei densities of $n_0 = 10^6$, 10^7, and 10^8 cm^{-3} at a time of 500 ns after the laser pulse. Laser parameters and material properties were as in Figure 8. Reprinted with permission from ref 55. Copyright 2002 American Institute of Physics.

can be interpreted as spall layers, although the prediction of a well-defined spall layer from the simple spallation model with a distinct tensile strength is obviously not valid. An important result of the simulation was that interacting bubbles collapse later than single bubbles because the pressure in the cavitating liquid is reduced below 1 bar. This explains the collapse times observed experimentally,[28] which for high values of radiant exposure exceeded the times calculated with a single-cavity model by almost a factor of 2.

C. Fracture and Ejection

So far the conditions for material fracture under stress have been discussed. If fracture is to cause ablation, a question remains about the driving force for ejection of the fragmented matter. In terms of energy conservation, the stress energy minus the energy required for fracture is, in principle, available to go into kinetic energy of the ablated fragments. This argument is equally valid for transient and quasi-static stress conditions.

For transient thermoelastic stress the ejection mechanism can be understood by looking at the one-dimensional solution of the wave equation. As stated above, the material in the vicinity of the free surface is accelerated to a maximum speed of p_0/Z_1 due to the reflection of the wave component p_2. Without fracture, the motion would stop and the surface would reach a new equilibrium position. If the material fractures at some depth below the surface, the motion continues and material between this depth and the surface is ejected. The formation of a spray dome due to reflection of a shock wave at a liquid surface has been described in a similar way.[56] The situation in liquids is somewhat complicated by the fact that in a later stage of ablation the collapse of large cavitation bubbles leads to strong hydrodynamic flow. Ablation may in this case be prolonged by the formation of liquid jets toward the free surface.[57]

Relatively few models exist that describe fracture including ablation. Among these are hydrodynamic codes and molecular dynamics simulations, which will be discussed next. A model for backplane and midplane spallation that includes ablation from the back surface based on a hydrodynamic code that includes material strength and failure was used by Glinsky et al.[58] Midplane spallation means that both sides of a target are simultaneously hit by laser pulses, causing a maximum of tensile stress right at the center plane. In the backplane spallation simulation it was assumed that a unipolar thermoelastic wave is generated at the interface of a transparent backing material and the absorbing liquid and causes spallation after reflection at the free back surface of the liquid. The front surface spallation process was not included in this study because the heating and resultant weakening of the material would have complicated the model. The model was able to predict the evolution of pressure and fractional void volume for different stages of damage. Experimentally observable time histories of back surface motion were calculated that showed the different stages of spallation, starting with an oscillation of the surface without failure, an overshoot without return to the initial position for void nucleation and, finally, ablation, characterized by a continued outward motion of the surface in the case of both nucleation and

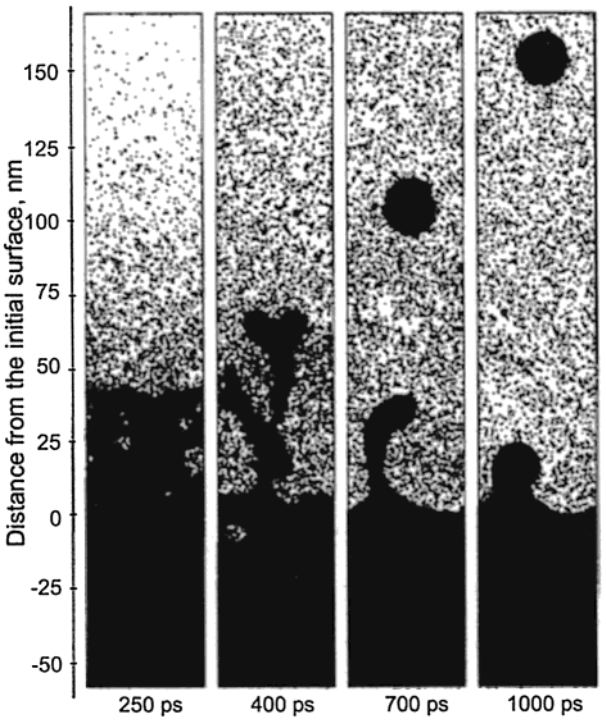

Figure 10. Snapshots from the molecular dynamics simulation of laser ablation of a molecular solid without stress confinement. The penetration depth of the laser radiation in the solid is 50 nm ($\mu_a = 2 \times 10^7$ m^{-1}). A laser having a wavelength of 337 nm, a pulse duration of 150 ps, and an incident fluence of 39 J/m^2 is assumed. Reprinted with permission from ref 60. Copyright 2000 American Institute of Physics.

failure. As the authors point out, the measurement of back surface position should provide quantities such as the tensile failure limit for nucleation and the failure strain for void coalescence. A similar model for front spallation of biological tissue was developed by Antoun et al. and will be discussed in the section on tissue ablation[59] (section IV.C).

A very complete model for ablation of organic solids was presented by Zhigilei et al. using a molecular dynamics simulation.[60] Details of this method can be found in a separate paper in this issue. The main purpose of this purely theoretical study was to demonstrate the influence of heat and stress confinement on the ablation process, which was done by comparing two different pulse durations, one shorter and one longer than the acoustic relaxation time and both shorter than the thermal relaxation time. For an absorption depth of 50 nm the characteristic times were $t_{ac} = 20$ ps and $t_{th} = 10$ ns, and the choice of pulse durations was 15 and 150 ps. In the simulations the onset of ablation was marked by a sharp transition from thermal desorption of molecules from the surface to collective ejection of larger masses at a threshold fluence, which amounted to 29 J/m^2 for 15 ps pulses and 35 J/m^2 for the 150 ps pulses. Apart from the lower threshold the ablation by shorter pulses was also initiated by a different physical mechanism, as revealed from snapshots of the ablated material (Figures 10 and 11). The longer pulses produced a phase explosion characterized by the ejection of a mixture of molecules and liquid phase clusters (Figure 10), whereas the shorter pulses first

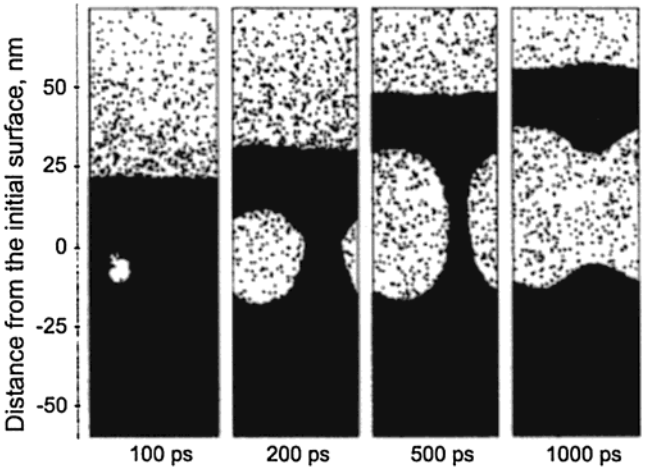

Figure 11. Snapshots of a molecular dynamics simulation of photomechanical ablation under conditions of stress confinement. Pulse duration = 15 ps, incident fluence = 31 J/m^2; other laser and material properties were as in Figure 10. Reprinted with permission from ref 60. Copyright 2000 American Institute of Physics.

initiated void nucleation below the surface, followed by their growth, coalescence, and finally the separation of a surface layer (Figure 11). This observation of photomechanical ablation was typical for a fluence value close to the ablation threshold. Below the threshold, the nucleation, growth, and collapse of single cavities was observed after irradiation with the shorter pulses. A comparison at a fluence value of 61 J/m^2, well above the threshold for a phase explosion, revealed that the shorter pulses still caused some photomechanically induced void nucleation below the surface, in contrast to the longer pulses that never produced subsurface voids. Also at this high fluence a higher ablation yield and the ejection of larger and more numerous clusters could be observed under stress confinement (short pulses) compared to thermal confinement alone (long pulses). The simulation was also used to calculate temporal stress profiles for both irradiation conditions. As expected, the maximum positive and negative stresses were much higher for the shorter than for the longer pulses. Under stress confinement, the positive amplitude of the bipolar stress wave (Figure 12) increased linearly with fluence, whereas the negative amplitude reached a peak value near the dynamic tensile strength. Higher fluence values yielded again smaller tensile amplitudes, which was attributed to thermal softening of the material, resulting in a lower strength, and to the increasing contribution of recoil momentum of the ejected mass.

IV. Photomechanical Ablation by Transient Thermoelastic Stress

A. Photomechanical Ablation Signatures

Whether photomechanical effects play a role in the ablation of a particular target is often difficult to decide. The typical indicator for photomechanical ablation is the fracture of the target material near the ablated surface. This fracture can be observed as the nucleation of voids or cracks in transparent

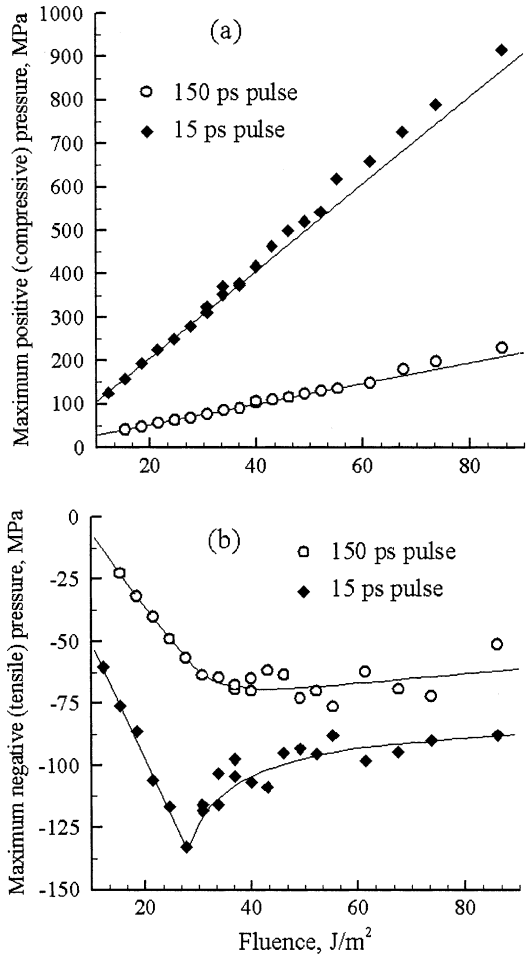

Figure 12. (a) Positive and (b) negative amplitudes of stress waves as a function of incident fluence calculated with the molecular dynamics code for a depth of 100 nm below the surface of a molecular solid. Different laser pulse durations are compared, with (t_p = 15 ps) and without (t_p = 150 ps) stress confinement. Other laser and material properties were as in Figure 10. Reprinted with permission from ref 60. Copyright 2000 American Institute of Physics.

materials but is difficult to observe directly in opaque materials. Other, indirect, indicators for photomechanical ablation are typical stress wave signatures under fracture and ablation, the characteristics of the ablation plume, and low ablation thresholds. We will first describe these characteristic signatures and will include typical results that apply to different materials. Specific, material-dependent photomechanical ablation signatures will be discussed in the later sections on ablation of liquids, biological tissue, and solids.

1. Cavity Dynamics

Cavitation, that is, the nucleation and growth of voids due to mechanical stresses, is the basic fracture mechanism in ductile materials and liquids. The dynamics of individual voids strongly influence the temporal evolution of the fracture and the following ablation. Time-resolved imaging has been used in several studies to study cavitation in transparent materials.[28,57,61−65] Under plane wave conditions cavitation is seen right above the compression−tension transition (Figure 13). In liquids or soft materials

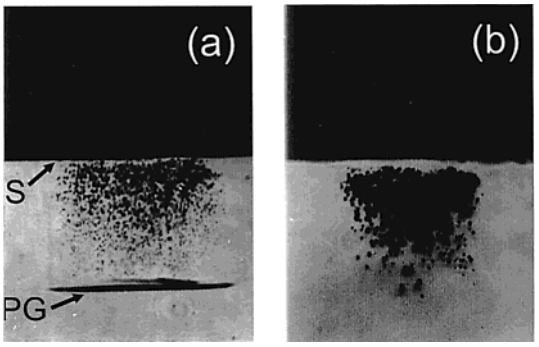

Figure 13. Flash photography of cavitation in water with μ_a = 19 cm^{-1} (a) 1 μs and (b) 10 μs after a laser pulse with a wavelength of 1064 nm, a duration of 8 ns, and a fluence of 3.5 × 10^4 J/m^2 has hit the liquid surface. The ambient pressure is 1 bar. The pressure gradient (PG) of the thermoelastic wave at the transition from positive to negative pressure is seen as a dark line in (a). The length of this line corresponds to the laser beam diameter of 2 mm. A cavity-free zone is formed directly below the surface (S).

such as biological tissue or gelatin the cavities first grow under the action of the tensile stress pulse and then collapse under the ambient pressure. The cavity lifetime is several microseconds, or even longer if coalescence takes place, and is usually much longer than the acoustic wave by which cavitation is driven. Directly below the free surface there is a more or less deep region where the tensile stress amplitude is too low to initiate cavitation. Only photographs in which this region is seen with high resolution can reveal this gap (Figure 13). At later times, usually a couple of microseconds after passage of the thermoelastic wave, cavities tend to accumulate in a more or less broad region at some distance from the surface, forming a "spall layer" (Figure 13). The fact that this layer is not well-defined contradicts the simple spallation model that assumes a distinct tensile strength but confirms the theoretical prediction of a broad cavitation zone from the more accurate molecular dynamics and hydrodynamic code calculations.[55,59,60] Time-resolved photography of cavitation in transparent tissue samples such as cornea or tissue phantoms such as gelatin yielded images of cavitation similar to those in liquids.[62,65]

Alternatives to time-resolved imaging are various optical pump−probe techniques. These offer the advantage that the complete time history of an event can be recorded, in contrast to single snapshots usually taken with imaging methods. Cavity dynamics have been investigated by measuring the scattering of a continuous probe light beam at single or multiple cavities using either transmission[28,63] or reflection[66] geometry. These experiments confirmed some of the findings from visual observation, such as the continued growth of cavities after passage of the thermoelastic wave. Growth and collapse were found to be almost symmetric in liquids (Figure 14a), whereas the more viscous properties of gels resulted in an asymmetric radius−time curve with a slower collapse than growth[28] (Figure 14b). Esenaliev et al. used the midplane spallation arrangement for studying cavitation in gels.[66] Apart from transient bubble clouds observed in the pump−probe experiment, they

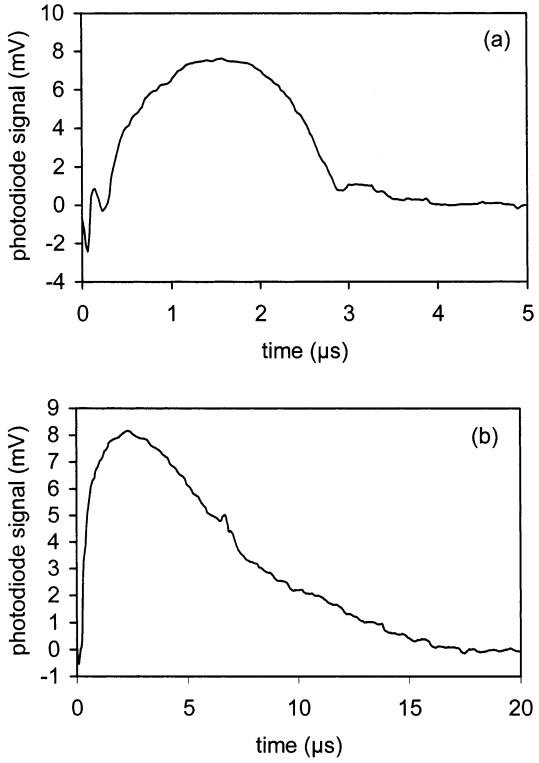

Figure 14. Pump−probe detection of cavitation in liquid (a) and gelatin (b) colored with Orange G after irradiation with a laser pulse having a wavelength of 532 nm and a duration of 8 ns. The curves show time-resolved transmission of a focused probe beam parallel to the sample surface at a depth z. A positive signal corresponds to a reduction of transmission due to cavitation. Signal in (a) water: $H_0 = 6.8 \times 10^3$ J/m^2, $\mu_a = 5000$ m^{-1}, $z = 300$ μm. Signal in (b) gelatin: $H_0 = 5 \times 10^4$ J/m^2, $\mu_a = 5000$ m^{-1}, $z = 200$ μm. Ambient pressure = 1 bar. Reprinted with permission from ref 28. Copyright 1996 Springer Verlag.

also found permanent void formation by microscopic inspection of the samples after irradiation. Paltauf and Schmidt-Kloiber used the front-surface spallation geometry and compared the experimental results from cavity dynamics in gelatin and liquid with theoretical simulations. The calculations were based on the motion of a single cavity driven by a thermoelastic transient.[28] The Gilmore model for cavitation in a viscous, compressible liquid was combined with a finite difference model for plane thermoelastic wave generation that took into account the finite laser pulse duration and the dependence of the Grueneisen parameter on temperature. Melting of the gelatin was taken into account by introducing a temperature-dependent viscosity. Radius−time histories of bubbles calculated with this model corresponded well with results from the optical pump−probe measurement as long as the cavity density was low. A discrepancy was found, however, in the case of high fluence, where high fractional void volumes were generated and the influence of bubble growth on the pressure could not be neglected any more. The hydrodynamic, self-consistent model by Strauss et al.[55] described earlier could accurately explain the prolonged lifetime of bubbles in this case. Another important result from the single-cavity model was that at depths $>1/(2\mu_a)$, where the tensile stress pulse is dominated by the component p_3 (eq 10), the bubble lifetime and maximum bubble size are determined by the radiant exposure, independent of the absorption coefficient. An analysis of the tensile stress history shows that when the absorption coefficient rises at constant radiant exposure, the stress amplitude rises but at the same time the duration of the stress pulse is decreased. This shows that a time integral over the pressure similar to the fracture criterion in eq 20 determines the cavity growth (Figure 15).

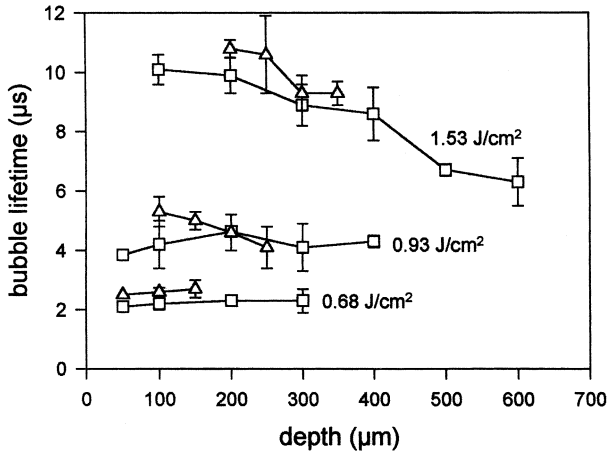

Figure 15. Cavitation bubble lifetimes as a function of depth in water measured with the optical pump−probe method from signals similar to those shown in Figure 14. Three different fluence values and two different absorption coefficients (squares, $\mu_a = 10000$ m^{-1}; triangles, $\mu_a = 5000$ m^{-1}) were used. Other experimental conditions were as described in Figure 14. Reprinted with permission from ref 28. Copyright 1996 Springer Verlag.

In opaque materials the void formation is not directly visible but can be indirectly observed by measuring the motion of the surface. Experiments on liquids and both hard and soft tissue samples have been performed using a Michelson interferometer setup.[67,68] The surface motion below the cavitation threshold was consistent with thermal expansion of the heated volume. At higher tensile stress amplitudes the generation of cavitation bubbles close to the surface caused a clear overshoot above the thermal expansion signal. This behavior corresponds to predictions from hydrodynamic models of back surface spallation.[58]

2. Stress Waves

Stress waves generated below the ablation threshold and their modification due to the onset of fracture and ablation give insight into the ablation mechanism and help to determine whether photomechanical contributions are present or not. Typically, the stress waves have an acoustic frequency spectrum ranging up to several hundred megahertz, making detection with high bandwidth necessary. Piezoelectric detectors made of poly(vinylidene fluoride) (PVDF) films[19] or lithium niobate[57] as well as various optical techniques based on interferometry[68] or time-resolved reflectance measurement[69] provide the necessary temporal resolution. With rising radiant exposure, other mechanisms besides thermoelastic stress contribute to the signals. These are gas formation by

thermal decomposition, ablative recoil momentum, and plasma generation.[70]

From theoretical models a characteristic signature of stress wave signals in the case of photomechanical ablation is expected. Hydrodynamic code calculations and molecular dynamics simulations predict that fracture and cavitation should primarily alter the tensile stress phase of the thermoelastic wave because a fragmented material can no longer support tension.[53,55,59,60] If fragmentation is accompanied by material ejection, this creates additional compressive stress due to recoil momentum. Different scaling laws for the peak recoil stress as a function of radiant exposure were found for the cases of rapid surface vaporization and explosive material removal.[7,71] In the former case, material ejection achieves a steady-state phase during the laser pulse and the scaling law becomes

$$\sigma_p \propto (H_0 - H_{th})^{2/3} \tag{30}$$

where σ_p is the peak stress and H_{th} is the threshold radiant exposure for ablation. Explosive material removal, on the other hand, starts after the laser pulse and is driven by the excess energy over the threshold value that has been stored in the target volume. The scaling of peak recoil stress with radiant exposure is in this case described by

$$\sigma_p \propto \left[\frac{2\rho H_0}{\mu_a t_p^{\,2}} \ln \eta \left(1 - \frac{1}{\eta} - \frac{\ln \eta}{\eta}\right)\right]^{1/2} \tag{31}$$

where $\eta = H_0/H_{th}$. Here it is assumed that the excess energy is converted into kinetic energy of the ablation products and that the recoil momentum per area, which is the time integral over the recoil stress, can be approximated by the product of the peak recoil stress and the laser pulse duration. Photomechanical ablation induced by material fracture is not included in these estimations but is expected to follow the scaling law for explosive ejection rather than that of surface vaporization. This is because under stress confinement conditions the generation of the tensile stress component starts after the laser pulse. The excess energy available for kinetic energy of ablation products is, however, in this case given by the stress energy minus the fracture energy, as mentioned above. Consequently, the maximum induced recoil stress cannot exceed the amplitude of the thermoelastic stress wave. This means that both the onset of fracture and the ablative recoil stress have the tendency to partly or fully cancel the tensile component of the thermoelastic stress wave. Because fracture without material ejection should not lead to any momentum being imparted on the target, the time integral over the stress wave must in this case vanish as it does below the fracture threshold. Experimental observations[28,52,53] and theoretical simulations[55] indicate that in the case of fracture or cavitation without material ejection, the tensile component is not only reduced in amplitude but at the same time prolonged until the collapse of the cavities. These changes have the effect that the time integral over the whole wave is kept at zero. Figure 16 compares thermoelastic stress signals in gelatin below and above the cavitation threshold. The signals are normalized for a better visualization of the change of shape that is caused by the cavitation. The positive part remains unchanged, but the negative part is strongly reduced in amplitude and shows an initial spike followed by a tail that is longer than the exponential decay of the undisturbed signal.

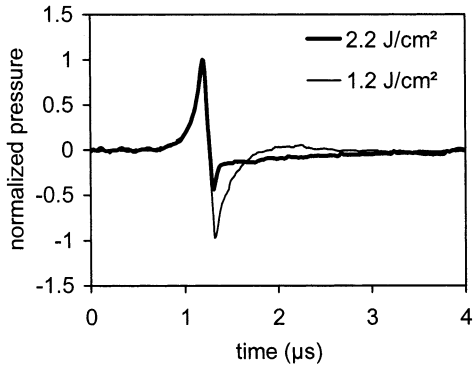

Figure 16. Normalized pressure signals generated by irradiating a gelatin target having $\mu_a = 1.1 \times 10^4$ m^{-1} with 8 ns long laser pulses. Signals below ($H_0 = 1.2$ J/cm^2) and above ($H_0 = 2.2$ J/cm^2) cavitation threshold are compared, showing the changes in the tensile phase due to cavitation.

The fact that fracture and recoil stress have similar effects on the shape of the thermoelastic stress wave makes it difficult to gain information about these processes from acoustic measurements alone. Although it is possible to attribute a reduction of the tensile wave to fracture if the total time integral vanishes and to the onset of ablation if the time integral gives a finite value, a sufficiently accurate stress measurement that is able to reveal the sustained tensile wave during the whole cavity lifetime is difficult. If with rising energy density other ablation mechanisms such as a phase explosion start to play a role, the ablative recoil stress can become higher than the thermoelastic stress, as now the energy available for material ejection exceeds the stress energy.

Various studies exist in which ablation stress wave signatures were compared at different degrees of stress confinement in biological tissue[7,71−73] and in polymers.[19,74] In these studies the samples were irradiated with different laser wavelengths to achieve a change of the absorption coefficient. With stress confinement satisfied, strong subthreshold signals could be measured with the typical bipolar shape. At high absorption where stress confinement conditions were not met, usually no signals could be measured below the ablation threshold, whereas the recoil stress above the threshold generated strong compressive signals.

Experiments under stress confinement conditions have been performed on liquids and soft tissue-like materials to find a correlation of changes in stress signals with cavitation and ablation thresholds.[57,61,63,75] The typical behavior of tensile stress in all studies was a linear rise with radiant exposure below the cavitation and ablation thresholds, a saturation at a certain level of radiant exposure followed by a return to the baseline (Figure 17). The latter is not predicted

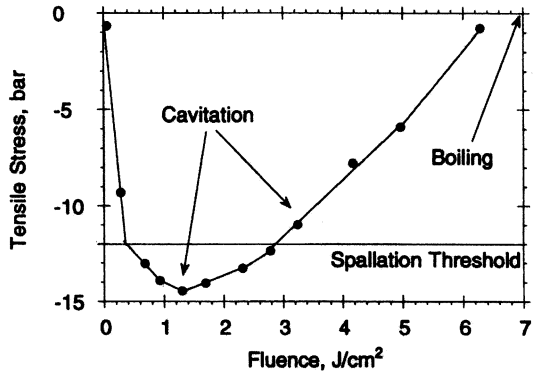

Figure 17. Amplitude of the tensile part of the bipolar thermoelastic wave measured in liquid as a function of incident fluence. An aqueous K_2CrO_4 solution with μ_a = 5500 m^{-1} at the laser wavelength of 355 nm was irradiated with laser pulses of 10 ns duration at an ambient pressure of 1 bar. A deviation from linear increase is seen at the cavitation threshold. According to the simple spallation model the tensile stress is expected to saturate at the spallation threshold (horizontal line). In reality the tensile amplitude approaches the baseline near the liquid boiling point. Reprinted with permission from ref 57. Copyright 1995 American Institute of Physics.

from a simple spallation model in which the tensile stress is rather expected to stay saturated at the cavitation threshold. At low absorption, where the stress signals are relatively long and their temporal profile can be measured with good resolution, a shortening of the tensile component in addition to its saturation was observable (Figure 16).[65] In some experiments the saturation of the tensile amplitude was observed at a calculated temperature equal to the boiling point.[75] Other studies, however, showed the same deviation from linear behavior at a much lower temperature (several degrees Celsius), where it was correlated with the cavitation threshold.[57] The reason for this discrepancy is not entirely clear but may lie in different contributions from acoustic diffraction in the experimental setups, which is known to increase the tensile relative to the compressive amplitude.[20] Another possibility is differences between the absorption coefficients of the samples used because increasing absorption requires higher radiant exposure levels to produce the same growth of cavitation bubbles.[28]

3. Ablation Threshold

The photomechanical ablation threshold should be higher than the threshold for photomechanical fracture because of the extra energy required for material ejection. At the same time the photomechanical ablation threshold is expected to be lower than the threshold for phase change induced ablation because of the much higher energetic efficiency of a fragmentation process compared to vaporization. This assumption, however, needs further discussion. Although fragmentation needs orders of magnitude less energy than vaporization, the energetic efficiency of thermoelastic stress generation is very low. The range of fluence values between the photomechanical and phase change-induced ablation thresholds may therefore be quite narrow if such a range exists at all. Looking, for example, at the theoretical prediction for organic solids based on molecular dynamics simulations (see section III.C) it can be seen that the threshold for phase explosion with 150 ps long pulses (stress confinement not satisfied) is only ~1.2 times higher than the threshold for photomechanically initiated ablation with 15 ps long pulses (stress confinement satisfied).[60]

To estimate the ablation threshold of a liquid, we can compare the thermoelastic stress energy Q_c from eq 15 with the minimum fracture energy Q_f, given by the energy for generation of free surfaces of droplets with radius s

$$Q_c = (A/4B)\Gamma^2\mu_a{H_0}^2 \qquad Q_f = (6V/s)\sigma_s \tag{32}$$

where V is the fractured volume. Setting $V = A/\mu_a$ and equating both expressions gives a value for $W_{th} = \mu_a H_{th}$, the minimum energy density that has to be deposited in the liquid under conditions of stress confinement to initiate fragmentation

$$W_{th} = (24B\sigma_s/\Gamma^2 s)^{1/2} \tag{33}$$

To generate water droplets with 10 μm radius therefore requires an energy density of 1.6×10^8 J/m^3 or 160 J/cm^3, corresponding to a temperature rise of ~38 °C. This rough estimation for brittle fracture neglects the temperature dependence of Γ and also that the initiation and growth of cavitation bubbles requires a certain favorable stress history. Nevertheless, it shows that photomechanical liquid ablation at moderate temperature rises is energetically possible. Indeed, the energy density range of pure photomechanical ablation below the boiling point has experimentally been found to be quite broad in liquids.[57,65] In biological tissue and in solids, however, experimental evidence for the existence of such a range is controversial. Also, there are quite inconsistent results regarding the relationship between ablation and fracture thresholds. Sometimes ablation thresholds clearly above cavitation thresholds were found,[65] whereas other studies revealed that these two thresholds virtually coincide or differ only slightly.[57,63] One reason for these discrepancies is that different experimental methods were used to determine thresholds. In some studies the stress wave signatures were used, and the ablation threshold was obtained from the onset of recoil momentum, measured from the time integral over stress signals. As mentioned above, the recoil measurement is based on the time integral over the stress wave signal that also strongly responds to the onset of cavitation, making it sometimes difficult to determine the cavitation and ablation thresholds independently. Time-resolved imaging is another method to observe the onset of ablation but has a qualitative aspect as it depends on subjective judgment to decide whether a laser pulse has produced ablation or not. Although this induces some uncertainty and makes it possible that very small amounts of ablated material are overseen, a definition of ablation as the collective ejection of a large mass of material implies that this should be easily visible with an imaging method that provides sufficient temporal and spatial resolution. Given that in photomechanical ablation the ablation

velocities are low and the material is ejected as more or less large fragments with sizes in the range of micrometers or tens of micrometers, visual observation should be an adequate method to measure thresholds in this case. Details on theoretical estimations and experimental findings regarding ablation and fracture thresholds will be given in sections IV.B−D.

A general trend specific to photomechanical ablation has been found regarding the dependence of the ablation threshold on the absorption coefficient of a sample. The energy density required for ablation increases with rising absorption coefficient, even if the stress confinement condition remains satisfied.[28,76] This observation has been explained as being the result of the influence of the stress history on the cavity dynamics. With a larger absorption coefficient the tensile phase of the thermoelastic stress wave becomes shorter, requiring a higher stress amplitude to achieve the same amount of cavity growth. Also, with shallower absorption depth the ejected fragments tend to become smaller, requiring a higher fragmentation energy according to eqs 23 and 32.

4. Ablation Plume

The hydrodynamic flow in the vicinity of the surface due to the incoming and reflected stress waves leads to the ejection of cold, intact fragments or clusters rather than of a mixture of liquid droplets and vapor as expected from a phase change induced ablation mechanism. This is interesting in the context of matrix-assisted laser desorption ionization (MALDI) because even large molecules can be desorbed from a matrix by use of photomechanical stress without being thermally fragmented. The ejection velocity is expected to be close to the flow velocity, as has been observed for liquid ablation.[65] Because this velocity is rather low, in the range of tens of meters per second, it can be used as an indicator for photomechanical ablation and to distinguish this from explosive photothermal ablation, where the ejection velocity can reach supersonic speed.[65,77]

B. Ablation of Liquids

Water is probably the most investigated liquid in the context of photomechanical ablation because it often serves as a model for soft biological tissue that contains ∼70−80% water. Furthermore, the thermal and mechanical properties of water are well-known. The maximum thermoelastic stress that is generated by heating water from room temperature to the boiling point is ∼1 kbar. This gives a 500 bar amplitude of the tensile stress wave, which should clearly exceed the heterogeneous and possibly also the homogeneous cavitation thresholds. Liquid ablation may also play a role in the photomechanical ablation of solids because heating of a solid might result in melting so that actually a liquid is fragmented and ejected.

A factor determining the ablation threshold of a liquid is the cavitation threshold. Time-resolved photography to visualize the gap between the free surface and the first layer of cavitation bubbles has been used to estimate this threshold under transient thermoelastic stress loading.[64] The width of the gap as a function of fluence together with the known values of Grueneisen parameter ($\Gamma = 0.11$) and absorption coefficient ($\mu_a = 2000\ m^{-1}$) yielded with eq 19 a cavitation threshold between −5 and −10 bar for water containing $CuSO_4$ as absorber for 1064 nm wavelength laser pulses.[64] This quite low threshold indicates heterogeneous cavitation. Inserting the experimental threshold values into Blake's formula (eq 27) gives for the corresponding size of nuclei, R_h, a value between 0.06 and 0.13 μm. Because the actual nucleation sites have a size distribution rather than a single size, this threshold value corresponds to the biggest nuclei in the liquid. Time-resolved stress detection with simultaneous observation using laser flash photography was employed by Oraevsky et al. to obtain a cavitation threshold for water stained with K_2CrO_4 ($\mu_a = 5500\ m^{-1}$) and irradiated with laser pulses of 355 nm wavelength and 10 ns duration.[57] The first appearance of visual cavitation bubbles and the onset of saturation of the measured tensile stress amplitude gave consistent values of −12 bar for the cavitation threshold. A similar value was found from an optical pump−probe measurement by Kim and co-workers[63] in an aqueous solution with $\mu_a = 55000\ m^{-1}$. Differences between the heterogeneous cavitation thresholds are partly due to the different impurity contents of the solutions. Much higher cavitation thresholds were observed in experiments in which cavitation was induced in the center of spherical liquid droplets with ∼100 μm radius by a radially converging, transient thermoelastic stress wave.[41] To induce cavitation bubbles in the center of the droplets, the tensile stress wave amplitude had to reach a value on the order of −500 bar. This high value can be attributed to the small interaction volume, making the presence of heterogeneous nuclei unlikely.

At fluence values only slightly above the ablation threshold the ablation plume consists of liquid droplets and jets that emerge from randomly distributed sites within the irradiated surface area.[57] At higher fluence, jets tend to become more numerous and to coalesce[28,65] (Figure 18). The random distribution of ejected jets and of droplet sizes has been attributed to capillary wave generation at the surface in an ablation model proposed by Golovlyov and Letokhov.[78] This model is based on the assumption that the spectral components of the thermoelastic wave near the surface have independent and random phases resulting in an acoustic speckle pattern. It is not clear, however, how the initially coherent acoustic field of the thermoelastic source should result in such a random distribution. Another more plausible explanation is that the fragmentation mechanism, which is in most cases the heterogeneous nucleation of cavitation bubbles, induces randomness into the ejection process. Typical liquid ejection velocities are in the range of tens of meters per second, consistent with the flow velocity in the vicinity of the free surface.[65] This first stage of ejection is followed after some tens or hundreds of microseconds by massive liquid jet formation, caused by the collapse of coalesced cavities.[57]

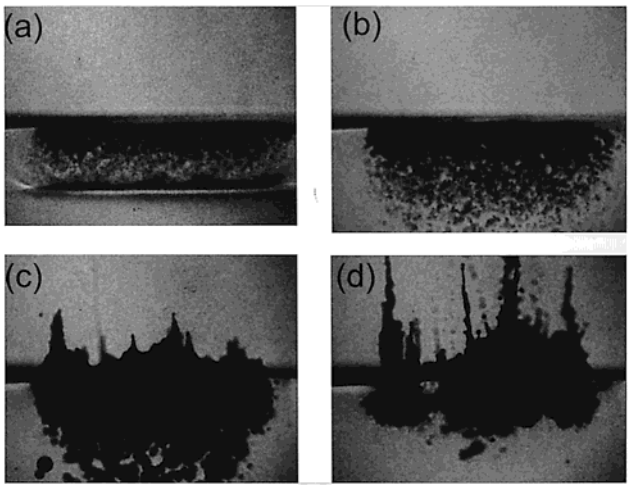

Figure 18. Sequence of images showing ablation of an aqueous dye solution with $\mu_a = 4200\ m^{-1}$ after irradiation with laser pulses having a duration of 8 ns and a wavelength of 532 nm. The fluence was $H_0 = 4.1 \times 10^4\ J/m^2$, giving an energy density of $W_0 = 1.72 \times 10^8\ J/m^3$ and a temperature rise of $\Delta T = 41$ °C. Delay times relative to the laser pulse: (a) 0.3 μs; (b) 1.1 μs; (c) 10 μs; (d) 30 μs. The diameter of the ablated area is 1.5 mm. Ambient pressure = 1 bar.

Various studies have shown that liquid temperatures at the ablation threshold under conditions of stress confinement lie clearly below the boiling point.[28,57,61,63,65,67] With rising absorption coefficient, however, threshold values have been found to approach the boiling point, which rather indicated a phase change-induced ablation mechanism.[75,77] The discrepancy may be partly due to the dependence of fragmentation and ablation threshold on the duration of the tensile stress pulse. An ablation threshold temperature below the boiling point has been found in benzene derivatives irradiated with UV lasers without stress confinement.[79] This behavior was attributed to a photochemical process.

The strong influence of the laser pulse duration on the liquid ablation mechanism has been demonstrated in studies that compared ablation with and without stress confinement conditions satisfied.[64,80] Short pulses led to photomechanical ablation accompanied by subsurface cavitation due to the transient thermoelastic stress. Using pulses much longer than the acoustic relaxation time resulted in liquid ejection as soon as the accumulated energy had raised the liquid temperature above the boiling point. In this case no subsurface cavitation was seen, but rather a hole caused by surface depression due to the recoil pressure of the ablated vapor plume.

C. Ablation of Biological Tissue

Soft biological tissue is a composite material, containing about 70% water and 30% biomolecules. Depending on the type of tissue, the mechanical properties are more or less determined by an extracellular matrix of collagen. Details about the composition and the mechanical properties of tissue can be found in the article on mechanisms of pulsed laser ablation of biological tissue by Vogel and Venugopalan in this issue. Stress confinement conditions can be easily obtained in tissue by laser sources that provide pulse durations of femtoseconds to nanoseconds. For example, with a pulse duration of 10 ns and a speed of sound of 1500 m/s the condition $t_p < 1/(\mu_a c_s)$ is satisfied if the absorption coefficient is $<6.7 \times 10^4\ m^{-1}$. Only in the deep UV where the absorption by the biomolecules is dominant and around the absorption peak of water at 2950 nm does the tissue absorption coefficient become higher than this value. On the other hand, if the absorption coefficient becomes too low, the laser fluence required to achieve sufficient thermoelastic stress amplitude for tissue fracture may become so high that plasma generation sets in, resulting in nonlinear absorption.[81,82] During picosecond or nanosecond laser pulses the rapid increase of absorption causes the energy density to rise almost instantly orders of magnitude higher than in the case of linear absorption, and the energy deposition becomes confined to a shallow region below the surface, where high temperature and pressure are achieved. Ablation is therefore limited to a very thin layer, even if the target is highly optically transparent. To stay in the linear absorption regime requires that the irradiance stays below the plasma formation threshold that for laser pulses shorter than a nanosecond has been observed[81] at irradiance values $E_0 = H_0/t_p$ around $10^{15}\ W/m^2$. For example, when a laser pulse with a duration of 10 ps is used to generate a thermoelastic stress amplitude of $\Gamma\mu_a H_0 = 100$ bar under linear absorption conditions, the absorption coefficient should be $> \sim 5000\ m^{-1}$ to avoid plasma formation. With ultrashort laser pulses in the femtosecond range the situation is different because the energy densities in the plasma are generally lower than with picosecond or nanosecond pulses and approach values that are achieved under linear absorption. Furthermore, with these short laser pulses the condition of stress confinement is achieved in the plasma region. Therefore, despite the different absorption mechanism, the plasma generation by femtosecond laser pulses results in very similar photomechanical effects as thermoelastic stress production under linear absorption.[83]

Ultimate tensile strength measurements of tissue for static stress have shown[84] that the strain at fracture can become very large, with values ranging up to ≈ 1. This is due to the composite structure of tissue. The components that provide tissue strength are collagen and elastin fibers, which under tensile loading first straighten and align with the applied stress before they are stretched themselves. Tensile strength values measured under static conditions cannot be readily applied to transient thermoelastic stress-induced fracture because here the strain rates may become quite high, reaching values of $\geq 10^5\ s^{-1}$. Various investigations have shown that as a general trend with rising strain rate the tensile strength of tissue increases.[85−87] Insofar as the initiation of cavitation and the void dynamics are concerned, it is expected that tissue will behave in a manner similar to a viscous liquid, owing to its softness at low strain. However, the final stage of photomechanical ablation, that is, the coalescence of voids and the

ejection of tissue fragments, is certainly determined by the composite structure and the high extensibility. Albagli et al. proposed a modification of the stress confinement principle for biotissues that includes the possibility of high strain at fragmentation.[5] Inertial confinement and high stress are assumed to be achieved if the laser pulse duration is shorter than the time until a strain of unity is reached in the absorbing volume at a certain strain rate, which depends on the deposited laser energy. Although the mechanism by which this strain rate is generated is not specified, predictions from this model agree well with the behavior of ablation threshold as a function of laser pulse duration.

The possibility that different tissue components provide mechanical strength and act as chromophore for the laser radiation has been analyzed by several authors,[7,88] who discussed possible consequences for the ablation mechanism.[89] If the chromophore is water, as in infrared laser-induced ablation, the generation of vapor bubbles can cause tensile stress in the extracellular tissue matrix, followed by fracture and photomechanical ejection, even if no stress confinement is achieved. In the case that the extracellular matrix is the target for absorption of laser radiation, as in the ultraviolet range, the structural integrity of tissue is weakened by photochemical decomposition and photomechanical ablation proceeds similarly to a homogeneous material, requiring stress confinement to generate sufficiently high tensile stress for fragmentation.

A model that includes the influence of the composite structure of tissue on the cavitation process was used by Antoun et al.[59] to describe front surface spallation of a collagenous tissue such as a cornea. Crossing points of collagen fibers were assumed to act as nucleation sites. A hydrodynamic code was used that had been originally developed for failure of metals and calculates the void size distribution under the influence of stress, starting at an initial exponential distribution given by eq 29. The void density n_0 (3×10^{14} cm^{-3}) was taken to be equal to the number of collagen crossing points and the size parameter R_0 (50 nm) equal to the size of collagen fibers. For an absorption depth $1/\mu_a$ of 3.7 μm the simulation yielded a maximum of void volume fraction at a depth of 2 μm, corresponding to the formation of a spall layer. However, the zone of increased fractional void volume extended to $\sim$5 μm. These results show again that the damage range is relatively broad, and the idea of defined locations of spall layers is not valid. The authors point out that for accurate modeling of the ablation a time- and temperature-dependent reduction of the yield strength should be incorporated in the model to describe the thermal softening of the material.

Quite different values for ablation thresholds of tissue and tissue-like materials such as gelatin have been reported by different authors. Thresholds similar to those of water, well below the phase change threshold (boiling point of water), were found by Oraevsky et al.[61] using total recoil measurements. In contrast, despite strong subsurface cavitation occurring, no ablation below the phase change threshold was seen by Paltauf and Schmidt-Kloiber,[65] who employed visual observation using time-resolved imaging. Aside from the different material properties (gelatin samples containing 5% dry gelatin powder in Oraevsky et al. and 25% in Paltauf et al.), this discrepancy might also be partly due to the different experimental methods employed.

Histological inspection of biological tissue after ablation sometimes reveals the contribution of thermal and mechanical effects to the ablation mechanism. Telfair and Hoffmann[90] attributed the minimal thermal damage zones after ablation of a cornea with infrared pulses from an optical parametric oscillator (OPO) to a photomechanical ablation mechanism.[91,92] The OPO generated pulses with a duration of 7 ns and a wavelength of 2.94 μm, where the absorption coefficient of tissue is $\sim 1 \times 10^6$ m^{-1}. Taking into account that the absorption coefficient at the energy density required for ablation is actually lower due to the temperature-dependent dynamical changes in water absorption,[93] a ratio $t_p/t_{ac} \approx 6$ is achieved. Under these conditions stress is not confined in the irradiated volume and the temporal profile of the thermoelastic stress wave follows the time derivative of the laser pulse profile. As it is pointed out in this study, despite the strong attenuation of the thermoelastic wave due to stress relaxation, the acoustic tension amplitude may achieve values at which the tissue could fracture mechanically.

D. Ablation of Solids

A great deal of work has been reported on the ablation of solids using deep UV excimer lasers and solid-state visible and near-infrared lasers as well as long wavelength infrared pulsed CO_2 lasers. Interest has centered on the removal of material for micromachining[94,95] and using the ablated material to grow films by ablation deposition.[96] All of the main groups of materials—metals, semiconductors, insulators, and polymers—have been encompassed in these studies. However, the extent to which photomechanical mechanisms contribute to and influence the ablation of polymers and other organic substrates is poorly understood as this topic has received relatively sparse attention.[97]

With pulses of nanosecond duration or longer, the conditions for neither thermal nor acoustic confinement are satisfied (eqs 1 and 4) for metals or for semiconductors if the photon energy is well above the band gap because of the small beam penetration depth. For organic polymers and inorganic insulators or semi-insulators, thermal confinement often applies but only rarely acoustic confinement, as the laser wavelength is usually chosen to match strong absorption bands in order to attain a low threshold fluence for ablation and precise depth resolution per pulse. Under these conditions $\tau = t_p/t_{ac} \gg 1$ and the amplitude of both the compressive and tensile components of thermoelastic stress waves is generally greatly reduced. A convenient analytical expression for the thermoelastic stress transient can be derived for an assumed laser irradiance variation of the form

$$E = E_0[1 - \exp(-kt)] \exp(-mt) \qquad (34)$$

where k and m define the rate of rise and fall of the pulse. E_0 is related to the pulse fluence H_0 by $E_0 = m(m + k)H_0/k$. The asymptotic form of the stress transient σ generated as a result of exponentially decreasing energy deposition with an absorption coefficient μ_a at a free surface when there is thermal confinement is then[98]

$$\sigma = -\frac{\mu_a \Gamma E_0}{2} \frac{k \exp(at')}{(m + a)(k + m + a)} \quad t' \leq 0 \quad (35)$$

$$\sigma = -\frac{\mu_a \Gamma E_0}{2}\left[\frac{2m \exp(-mt')}{m^2 - a^2} - \frac{2(m + k) \exp[-(m + k)t']}{(m + k)^2 - a^2} - \frac{k \exp(-at')}{(m - a)(k + m - a)}\right] \quad t' > 0$$

Here $t' = t - z/c$, where z ($\gg \mu_a^{-1}$) is the distance from the irradiated surface to the receiving plane of the stress wave and $a = \mu_a c_s$.

We can consider two limiting cases:

(i) When $k,m \gg a$ and there is acoustic confinement, both the compressive and tensile amplitudes of the stress transient are maximum with values

$$|\sigma_{max}| = \mu_a H_0 \Gamma/2 \quad (36)$$

which corresponds to the expression used earlier for the pressure amplitude of a one-dimensional thermoelastic wave in a liquid. Here the precise shape of the excitation pulse is immaterial and an essentially symmetric bipolar wave is produced. The condition on m and k is quite stringent if the maximum negative stress is to develop and requires $m \approx k > 10a$. Taking, for simplicity, a pulse with $m = k$, the laser pulse duration (full width at half-maximum) is $t_p = 1.9/m$, and to satisfy $m \geq 10a$ requires $\mu_a \leq 0.19/c_s t_p$. With $t_p = 15$ ns as typical of a "nanosecond" excimer or solid-state laser and $c_s \approx 2500$ ms^{-1} for the velocity of bulk waves in a polymer, the absorption coefficient should be <5070 m^{-1}. This is much smaller than encountered in most nanosecond laser ablation experiments where, as noted above, μ_a is preferably large and will typically be 10^6–10^7 m^{-1} for polymers and insulators. For metals the effective energy deposition range is governed by heat diffusion and, for nanosecond pulses, is of the order of a micrometer or so (i.e., equivalent to a $\mu_a \approx 10^6$ m^{-1}). An example of a thermoelastic signal generated in poly(methyl methacrylate) (PMMA) by a 308 nm XeCl laser is shown in Figure 19 and corresponding modeling results using eq 35 in Figure 20a. In this case of weak absorption ($\mu_a = 1500$ m^{-1}), the stress confinement condition is satisfied, resulting in a characteristic symmetrical bipolar pulse.

(ii) For conditions such that stress waves propagate out of the deposition zone on the same time scale or faster than the energy deposition time, that is, $k,m \leq a$, the magnitude of σ is greatly reduced. For example with $k = m = 0.05a$ and $t_p = 15$ ns, the peak compressive stress becomes $3.5 \times 10^{-3}\ \mu_a H_0 \Gamma$ and is much smaller compared with the stress confinement case in (i) above. The reduction factor is even more severe for the tensile component, as can be seen from Figure 20b, where the stress σ calculated using eq 35 is shown versus t'. This is because the pulse shape defined by eq 34 has a slower fall than rise time.

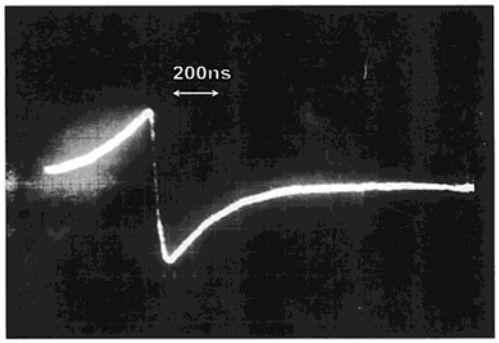

Figure 19. Thermoelastic stress wave signal recorded using a PVDF film transducer for PMMA irradiated with the 308 nm XeCl laser. Laser pulse duration $t_p \approx 24$ ns, fluence $H_0 = 2 \times 10^3$ J m^{-2}, PMMA absorption coefficient $\mu_a \approx 1500$ m^{-1}.

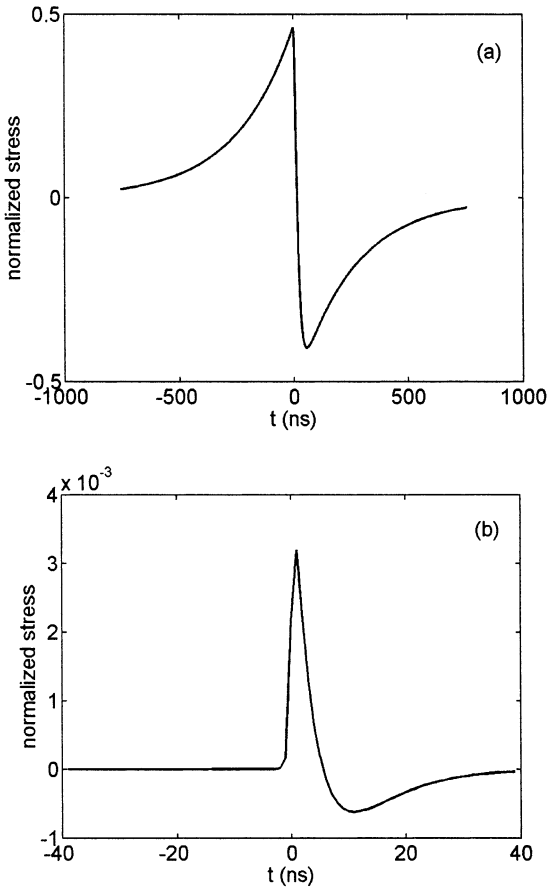

Figure 20. (a) Calculated thermoelastic stress wave signal generated in a sample with $a = \mu_a c_s = 3.97 \times 10^{-3}$ ns^{-1} and $m = k = 0.0792$ ns^{-1} chosen to model PMMA irradiated with a 24 ns duration XeCl laser pulse (see Figure 19). The normalized stress, $\sigma/(\Gamma \mu_a H_0)$, is shown versus the time in nanoseconds. Compressive stress is shown with positive sign. (b) As above but with $a = 2.53$ ns^{-1} and $m = k = 0.126$ ns^{-1} (15 ns pulse duration) to illustrate a stress signal when the acoustic confinement condition is not met.

The volumetric energy density loading, $\mu_a H_0$, determines the magnitude of σ in the above expressions. This too plays a crucial role in determining the threshold for the onset of significant ablation from a material surface, whether this occurs through a volume process as in polymer decomposition or a classical surface vaporization in metals or semiconductors. With the inception of ablation large compressive stress can be generated in the target surface as a result of momentum transfer (reaction force) produced by the ablating species. This can be of sufficient magnitude to easily cancel tensile thermoelastic components in the surface. The ceiling on $\mu_a H_0$ set by ablation (i.e., the ablation enthalpy) is of the order of 3−4 GJ m^{-3} for polymers and roughly 10 GJ m^{-3} for metals when significant surface vaporization commences.

Using eq 36 the maximum tensile component of the stress wave is predicted to exceed the failure strength of PMMA (tensile strength ~ 55 MPa under quasistatic conditions, $\Gamma = 1.12$) at an energy density loading $\mu_a H_0 \geq 0.1$ GJ m^{-3}. This is well below the ablation enthalpy. For a sample with $\mu_a = 5000$ m^{-1} at the XeCl laser wavelength,[99] where stress confinement approximately applies, this would correspond to a fluence of $\sim 2.0 \times 10^4$ J m^{-2} and irradiance of 1.3×10^{12} W m^{-2} for $t_p = 15$ ns. It is thus feasible that photomechanical damage may be responsible for ablation in undoped PMMA at 308 nm.[99] The reported thresholds for this vary, probably because of differences between the μ_a values for samples used by different workers, but are in the range of $\sim 1.1 \times 10^4$ and 3×10^4 J m^{-2},[99−102] within which the above estimate falls. The ablation craters reported in these experiments are typically described as exhibiting rough edges and cracking, which is the type of "fractured" morphology that might be expected if removal was driven by a nonthermal mechanical mechanism. The surface temperature rise, estimated from $\Delta T = \mu_a H_0 / \rho C$ as 13−84 K, depending on the incident fluence and μ_a, is insufficient to raise PMMA through its glass temperature, so it would remain brittle and thus susceptible to cracking. However, as noted in section II.B the peak tensile stress is not reached at the surface of the material and is only $0.86\sigma_{max}$ at a depth into the surface of μ_a^{-1}. It is thus difficult to explain the removal of shallow layers (depth $\ll \mu_a^{-1}$) by this one-dimensional stress generation mechanism.[25] In these experiments on PMMA the aspect ratio (beam radius/penetration depth) is small and the full three-dimensional analysis of thermoelastic stress reported by Albagli et al.[24,25] is needed. Under these conditions transient and quasistatic tensile stress develops close to the surface and may explain the "photomechanical" removal of shallow layers. It must be recognized that other "nonthermal" mechanisms such as field-induced breakdown and plasma formation at the surface or within the bulk of the polymer could be involved at the irradiance levels used. If this was the case, then the nature of the damage could equally well be explained by shock waves driven by the high-pressure plasma.

For a polymer irradiated at a wavelength where it absorbs strongly so that, for example, $\mu_a = 10^7$ m^{-1}, stress confinement would need pulses shorter than ~30 ps. Using the example of PMMA, mechanical failure would be predicted at fluences of $>10^4$ J m^{-2} or an irradiance $>3 \times 10^{14}$ W m^{-2} for a 30 ps pulse. As an optical breakdown plasma would almost certainly set in well below this irradiance level and become the dominant "ablation" mechanism, photomechanical effects are unlikely to be influential in this regime. We note, however, that Hare et al.'s[97] studies of dye-doped PMMA layers with 150 ps laser pulses imply that stress-induced ablation can coexist with thermochemical ablation. In their work consideration is also given to changes in the mechanical properties of PMMA above its glass temperature, which can influence the dynamics of the interaction through alteration of the sound speed and viscous contributions. It must be concluded that, even for a relatively simple material, the interaction is complex and may involve more than one ablation mechanism.

These examples serve to illustrate several important points.

- For nanosecond or longer duration laser pulses the magnitude of the tensile stress wave is generally small, except when the material is weakly absorbing. In most ablation experiments on organic polymers with these lasers, photomechanical contributions to removal appear to be unlikely.
- In polymers for which the laser wavelength is chosen to match strong absorption bands so that $\mu_a \gg 10^5$ m^{-1}, high-amplitude tensile stress generation is the domain of picosecond duration lasers. This is similarly the case for metals and for semiconductors and inorganic compounds when the laser matches strong absorption bands.
- At energy density loadings at which photomechanical effects could conceivably induce damage in these materials, ablation will usually have commenced and tensile stress will by over-ridden by compression waves generated by recoil momentum.

E. Transient Thermoelastic Stress and Phase Explosion

Thermoelastic stress-induced fragmentation of a material is the primary mechanism for purely photomechanical ablation below the fluence threshold for a phase explosion. It has been shown, however, that if stress confinement conditions are satisfied, photomechanical fragmentation plays also a role above the phase explosion threshold. Such an ablation mechanism can be regarded as photomechanically triggered vaporization. Figures 21 and 22 show snapshots from ablation under these conditions, comparing a molecular dynamics simulation for an organic solid[60] with an experiment in water. The process of photomechanically assisted vaporization is characterized by subsurface fragmentation and high ejection velocities.

In this ablation mode the transient thermoelastic stress plays a minor role in the material ejection, which is caused by the expanding vapor rather than by the hydrodynamic flow in the acoustic wave. However, the tensile part of the thermoelastic stress

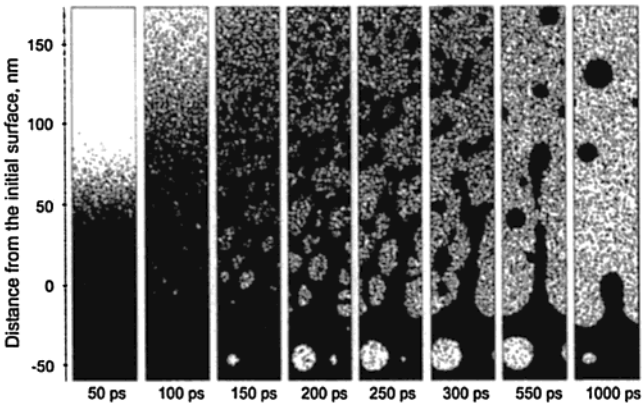

Figure 21. Molecular dynamics simulation of ablation of a molecular solid under conditions of stress confinement above the phase explosion threshold. Sample absorption coefficient = 2×10^7 m^{-1}, laser pulse duration = 15 ps, incident fluence = 61 J/m^2. Reprinted with permission from ref 60. Copyright 2000 American Institute of Physics.

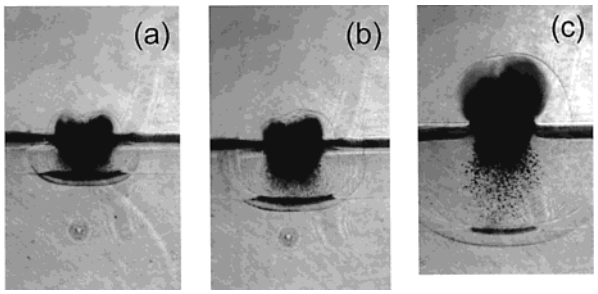

Figure 22. Series of photographs showing ablation of liquid under stress confinement conditions. An aqueous $CuSO_4$ solution with $\mu_a = 1900$ m^{-1} at the laser wavelength of 1064 nm was irradiated with 8 ns long pulses. The incident fluence was 2.6×10^5 J/m^2, giving a maximum estimated temperature of 140 °C. The ambient pressure was 1 bar. Delay times after the laser pulse: (a) 300 ns; (b) 550 ns; (c) 1000 ns. The laser spot diameter was 1 mm. The liquid surface is seen as a horizontal line, and the laser pulse is incident from the top of the images. The pressure gradient at the transition from compression to tension is seen as a dark line propagating downward from the surface.

transient triggers the phase change as seen in the sequence of experimental images in Figure 22, where nucleation is seen above the transition from compression to tension. In this experiment, the water was heated under conditions of stress confinement to a temperature of 140 °C. The states in the $p-V$ plane achieved in the medium under these conditions are shown in Figure 23. The heating (transition A → B) without volume change results in a state of high positive pressure outside the phase change region. When the negative pressure wave arrives, the material undergoes a rapid change of state into the metastable range and may even reach the superheat limit at the spinodal (as indicated by state C in Figure 23) where $dp/dV = 0$. At this state strong nucleation sets in and initiates explosive boiling. The onset of boiling and ablation is delayed until the transition from positive to negative stress, which always occurs after the end of the laser pulse if stress confinement conditions are obtained. Without stress confinement, this transition occurs during the falling

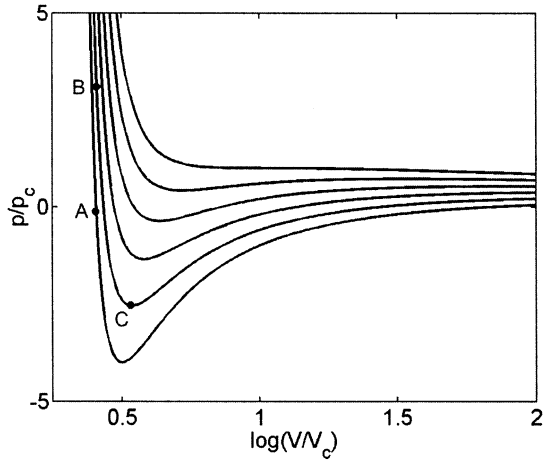

Figure 23. Transitions in the $p(V)$ plane during heating under stress confinement conditions (A → B) and at the arrival of the tensile stress pulse (B → C). A few van der Waals isotherms are depicted, with pressure and volume normalized to their critical values.

slope of the laser pulse, enabling the start of the phase explosion before the end of the laser pulse, yet at a higher temperature.

V. Diagnostic Applications of Laser-Generated Stress Waves

Stress waves generated in the subablation threshold thermoelastic regime and by the recoil momentum when ablation occurs can provide a variety of useful pieces of information on the laser interaction mechanisms for organic polymers and biological materials.[19,70,73,98] As is evident from eq 35, the rise time of the leading edge of the stress wave ($t'' < 0$) is given by $(c_s\mu_a)^{-1}$ so that if c_s is known, the absorption coefficient μ_a can be determined. The trailing edge of the tensile wave can likewise be used if t_p is sufficiently short compared to $(c_s\mu_a)^{-1}$. The limiting factor is then the electrical time response τ_{el} of the system used to detect and display the stress waves, which must be considerably shorter than $(\mu_a c_s)^{-1}$ to faithfully determine μ_a. For simple thin film piezoelectric transducers with τ_{el} on the order of a few nanoseconds, this restricts μ_a to $< 1.8 \times 10^5$ m^{-1} for biological samples[98] and to about half this value for polymers where c_s is higher. It is also necessary to use laser spot sizes that are large compared with μ_a^{-1} and a short propagation distance to the transducer to ensure validity of the one-dimensional thermoelastic model and negligible acoustic diffraction effects. The method has proved to be useful for biological tissues,[73,103−105] where both absorption and scattering may contribute to attenuation (i.e., the effective value for μ_a) and can also allow incubation effects associated with laser-induced changes in absorption to be investigated.

For polymers exposed to UV excimer laser pulses in air, the nature of the stress transient produced below the threshold for ablation was found in ref 19 to depend on the absorption coefficient. For strongly absorbing materials such as polyimide and poly(ethylene terephthalate) (PET) irradiated at 193 nm, it was reported that short duration compressive stress pulses rather than the characteristic bipolar

thermoelastic pulses persisted below the ablation threshold. This was tentatively explained by the fact that in this case there is little stress confinement (i.e., $\tau = t_p/t_{ac} \gg 1$), so the stress magnitude is greatly diminished, and recoil momentum produced by a low level of material "desorption" from the surface could mask the tensile component.[19] Characteristic thermoelastic signatures were seen, however, for PMMA and polyethylene irradiated with the 193 nm ArF laser and PMMA and PET with the 308 nm XeCl laser, confirming that relaxation of photoexcited states to produce heating occurred on a time scale that was short compared with the laser pulse.[19] Zweig et al.[70] made a detailed investigation of stress wave generation in polyimide exposed over a wide range of fluence ($30-10^6$ J m^{-2}) using the 351, 308, 248, and 193 nm excimer laser wavelengths. On the basis of the observed fluence scaling and temporal signature of the stress waves they deduced that product expulsion through thermal decomposition was the main mechanism contributing to stress at 351 and 308 nm in the subablation threshold regime. For low radiant exposures with the 248 and 193 nm lasers, however, they concluded that photochemical bond breaking might be important.

The compressive stress waves generated at fluences exceeding the threshold for significant ablation were found by Dyer and Srininasan[19] to commence within a few nanoseconds of the start of the laser pulse, indicating that the UV laser-induced polymer decomposition mechanism is rapid. These findings were later challenged by Kukreja and Hess,[106] who reported that compressive stress pulses in polyimide ablated with the XeCl laser were delayed by several hundred nanoseconds with respect to the start of the laser pulse. Only at high fluences did they observe prompt ablation. Experiments at longer wavelengths, using a transversely excited atmospheric pressure (TEA) CO_2 laser with $t_p \approx 110$ ns tuned to the 9 μm band to ablate PET, revealed characteristic bipolar thermoelastic stress wave formation below the ablation threshold.[107] When the fluence was raised, the tensile component of the stress became overtaken by a compressive pulse attributed to ablation recoil and lasting for several hundred nanoseconds. It has been observed that the amplitude of stress waves is dependent on temporal substructure within the CO_2 laser pulse. For example, high-frequency ($\sim$160 MHz) thermoelastic waves driven in PET by the nanosecond pulse train of a spontaneously mode-locked TEA CO_2 laser resulted in peak stresses of $\sim 10^6$ Pa.[108]

Although only a small mass of material is removed from the polymer surface by each laser pulse in ablation, the associated recoil stress can be large, reaching in excess of 10^7 Pa (100 bar) for exposure at several times the threshold fluence.[19] The magnitude, σ_A, of this stress can be estimated from the recoil momentum of the expelled products[98]

$$\sigma_A = V_e \rho (ds/dt) \tag{37}$$

where V_e is the velocity of material expelled from the surface and ds/dt is the surface recession velocity. The material is assumed to ablate layer-by-layer, and accelerative terms in the flow are neglected. If the material has an ablation threshold H_{th} and obeys a Beer's law ablation depth dependence of the form $s = \mu_a^{-1} \ln(H_0/H_{th})$, eq 37 becomes

$$\sigma_A = 0 \qquad \int E\, dt \le H_{th} \tag{38}$$

$$\sigma_A = \frac{V_e \rho E}{\mu_a \int E\, dt} \qquad \int E\, dt > H_{th}$$

For the simple case of an exponentially falling laser pulse of the form $E = E_0 \exp(-mt)$ (eq 34 with $k \to \infty$) we obtain

$$\sigma_A = \frac{m V_e \rho}{\mu_a}\left(\frac{H}{H_{th}} - 1\right) \tag{39}$$

Taking a polymer with $\rho = 1200$ kg m^{-3}, $\mu_a = 5 \times 10^6$ m^{-1}, a typical speed for the expelled ablation products of 10^3 ms^{-1} and $1/m = t_p = 15$ ns, a peak stress of $\sigma_A = 1.6 \times 10^7$ Pa is found at $H/H_{th} = 2$, that is, twice the ablation threshold. This simple modeling thus gives order of magnitude agreement with typical experimental findings. As V_e in eq 39 will vary with fluence, σ_A will, in general, be a nonlinear function of H.

In some cases,[70,73,98] it has been found possible to determine the ablation threshold by plotting σ_A versus H, as there is a distinct change in the slope when ablation starts. In Zweig et al.'s studies of polyimide, the fluence range encompassed not only the "ablative" regime where expelled products are principally neutral but also that where a plasma is initiated at the sample surface.[70] Under the latter conditions they measured peak compressive stress as high as $\sim 10^9$ Pa at 10^6 J m^{-2}. In a related study Zweig and Deutsch[109] used the 308 nm XeCl laser to ablate polyimide targets covered with water, a situation analogous to that often encountered in tissue ablation. Using an optical probe, they measured high Mach number propagation speeds for the stress waves formed in the water, implying that large amplitude shock waves (>10 kbar) are generated under these conditions. They attributed this to the confining effect the liquid has on the gaseous products of ablation, the peak stress being significantly enhanced, even at quite low fluences. Clearly, by momentum conservation correspondingly intense compressive stress waves will be launched into the solid.

It has been shown above that compressive stress generated by recoil momentum can be used to analyze the laser interaction mechanism. In this context the question arises whether this compressive stress itself may be responsible for further damage and fracture of the target material. There is no real evidence that compressive stress at the (unconfined) surface of an ablating polymer influences the material removal process or that compressive stress waves propagating within the polymer bulk cause material damage. An effect might arise if acoustic impedance mismatch at the rear sample surface gave $R_{ac} = -1$, causing a reflected tensile stress pulse to fall on the irradiated surface while this was still hot. The effect, if any, of this does not appear to have been investi-

gated. Matters are different for short-pulse laser ablation of tissues, as biological systems are much more susceptible to damage by stress pulses and effects may be complicated because of the heterogeneous nature of the medium through which the waves propagate. Of particular significance is that stress pulses can inflict biological "damage" at a range well beyond the laser absorption depth, μ_a^{-1}. Stress transients have, for example, been suggested as contributing to the spallation of endothelial cells in the cornea when excimer laser cuts are terminated close to the rear surface.[110] Ablation-induced stress and acoustic impedance mismatch at the posterior of the cornea are the proposed mechanisms. It is known from experimental studies that short pulses of compressive stress are generated when the cornea is ablated using the ArF laser.[72,73] The stress amplitude increases rapidly above the ablation threshold of $\sim$500 J m^{-2}, the magnitude reaching values of $\sim 10^7$ Pa, which is similar to those found in polymer ablation.[73] Studies of cell injury in skin ablated with the ArF laser in air[12] and under water[111] have been reported and provide evidence that photoacoustic transients may be implicated in disrupting cells well beyond the beam penetration depth and the range over which radical diffusion can occur.

Work has also been reported on the ablation of inorganic materials. For example, stress wave measurements of KrF laser ablation of the high-temperature superconductor YBCO were used to deduce the mean mass of species expelled from the surface.[112] This mass was considerably higher than expected for conventional surface vaporization, suggesting that removal took place by a "volume" mechanism involving explosive superheating (i.e., a phase explosion).[113] More recently, stress wave measurements have been used to test the validity of a model for transient surface vaporization of aluminum under laser heating with pulses in the 7−16 ns range at 1064 and 532 nm.[114] In these studies nanometer-scale displacement of the rear surface of the sample was detected using a stabilized Michelson interferometer, and the results were compared with theoretical predictions of the induced stress/strain.

The application of laser-generated stress waves in the field of nondestructive testing is now well established,[115] and the characteristics of both the thermoelastic and ablative generation regimes as ultrasound "sources" are relatively well understood, particularly for metals.[114,116] Various elastic moduli can be derived by measuring bulk and shear stress wave propagation velocities,[117] the laser-based method having the advantage of requiring only small sample size and, with optical detection,[115] being totally noncontact. Basic acoustic and mechanical properties of crystals,[118,119] anisotropic polymer-carbon fiber composites,[120] and superconductors[112] have been determined in this fashion.

VI. Photomechanical Ablation of Layers

The laser ablation of thin layers on substrates is of considerable interest as it has technical applications in low threshold film patterning and data recording,[26] forward transfer for patterned film deposition,[9] and molecular implantation.[121] Although, in many of these cases, removal appears to be driven largely by the pressure generated by a vaporized phase of the material, there is evidence that photomechanical effects may play a role under certain circumstances. Examples of this include what have been termed shock-induced ablation[97] and stress-induced ablation.[26]

Shock-induced ablation was investigated by Hare et al.[97] for dye-doped PMMA films of a few micrometers thickness on a glass substrate irradiated using 150 ps duration pulses from a 1.064 μm YAG laser. Coherent Raman scattering was used to determine the temperature and pressure in the layer providing quantitative information on the conditions under which ablation took place. With this short laser pulse there is stress confinement resulting in large amplitude tensile waves being generated. The authors deduced from their measurements that, at the threshold for ablation, roughly equal contributions to the pressure in the film came from "shock" and thermochemical decomposition of the polymer. They discuss film ejection in terms of a tensile stress wave generated at the acoustic mismatch between the film and substrate interface. Experiments on stress-induced ablation of Ti and TiN coatings on a glass substrate were reported by Koulikov and Dlott,[26] using a range of 1.064 μm YAG laser pulse lengths (1 ns−10 μs). They observed low ablation thresholds and interpreted this in terms of the release of (quasi-static) thermoelastic stress energy generated in the laser heated layer. The authors[26] use an energy criterion similar to that of Grady's[13] for homogeneous materials to model the ablation of the absorbing coating. This has a higher thermal expansion coefficient than the substrate and is heated by a laser pulse that is much longer than the acoustic relaxation time. Due to confinement in the radial direction by the surrounding cold film, stress energy builds up that opposes the thermal expansion. To initiate removal, the stress energy in the heated film must, at minimum, exceed the adhesive energy to the substrate and cohesive energy between the disk perimeter and surrounding film. A sudden release of stress energy at the moment of fracture causes ablation, the excess thermoelastic stress energy thereby appearing as kinetic energy of the ablated coating. This publication is probably one of the few, if not the only one, that demonstrates photomechanical ablation due to quasi-static thermoelastic stress. It seems likely, though, that this mechanism may, to some degree, be contributory in other film−substrate systems.

VII. Photomechanical Effects in MALDI

The technique of MALDI mass spectrometry has found very widespread use in the analysis of macromolecules and biomolecules.[122] The analyte is incorporated in diluted form in a laser-absorbing matrix that is usually a semicrystalline solid (e.g., 2,5-dihyroxybenzoic acid, ferulic acid). When this is irradiated at modest laser fluence ($\geq$100 J m^{-2}), the matrix is vaporized along with intact ions of the analyte, allowing their detection and analysis by a time-of-flight mass spectrometer. It has been found

to be possible to implement successful MALDI analysis using various short pulse lasers (usually a few nanoseconds to a few hundreds of nanoseconds) with wavelengths ranging from the ultraviolet (UV) through infrared (IR), although most commonly the 337 nm N_2 laser is employed.

At the mechanistic level there remains a puzzle in MALDI as to how very large molecules can be vaporized from what is predicted to be a relatively hot surface without undergoing extensive fragmentation and how they become ionized. Many explanations have been put forward, including models related to mechanical fragmentation[122,123] and laser-induced acoustic desorption[124] that are relevant within the context of the present review. The possibility that laser-induced thermomechanical stress contributes to the disintegration of MALDI matrices with IR lasers, where beam penetration in the matrix is deeper than with UV lasers, was put forward by Beavis et al.[125] and elaborated upon by Vertes and Levine.[126] The basis of this suggestion appears to be earlier experimental studies on the laser desorption mass spectrometry of nonvolatile molecules reported by Lindner and Seydel.[127] In this work the authors used samples of thermally labile oligosaccharides that are sensitive to thermal decomposition, mixed with NaI or KI. The experiments used a 10 ns duration frequency quadrupled (265 nm) Q-switched Nd:YAG laser focused to a small focal spot on thin ($\sim$1 μm) and thick ($\sim$ 20 μm) solid samples at high irradiance levels (1×10^{12} and 1×10^{15} W m^{-2}). Species entered the mass spectrometer from the rear sample surface viewed in the direction of the incoming laser beam. For thin samples, where the laser perforated the sample, the mass spectra of "desorbed" species revealed that extensive fragmentation of the molecules (e.g., raffinose and sucrose) occurred. In contrast, for thick samples, where there was no perforation and hence no possibility of direct injection from the (hot) ablation "plume", intact molecular ions of the sample could still be detected and in fact were predominant, the extent of chemical fragmentation being much reduced. The authors postulated that a shock wave generated at the front surface penetrated the sample leading to the desorption of intact molecules at the rear side through vibrational disturbance of the molecular binding potential. In view of the magnitude of forces that are attainable on small particles even under extreme conditions of deceleration (see Photomechanical Effects in Laser Cleaning, section IX), it seems unlikely that molecules can be directly "desorbed" in this way. It is more likely that molecular release associated with spallation fracture of the solid is involved. Experiments were also carried out with a layer of alkali salt on the rear of the samples and showed that ionized alkali ions were produced in the "shock" wave mode. It was suggested that postdesorption gas-phase reactions between these and the organic molecules might be responsible for the formation of the quasi-molecular ions that were detected.

More recently, Golovlev et al.[124] have reported modeling and experimental studies of laser-induced acoustic desorption (LIAD) resulting from unloading waves produced at the rear surface of a target. They propose LIAD as an efficient way of achieving "soft" desorption of large molecules for mass spectral studies. It is argued that the spectrum of acoustic waves generated with short pulse lasers can match well with characteristic frequencies of molecule−surface bonds but not with intramolecular vibronic bonds so that desorption can occur without fragmentation. Modeling of the phase space trajectory of particle motion induced by an acoustic pulse is discussed, although no quantitative details are provided. Their experimental arrangement used two, 2 mm thick, sapphire plates to sandwich a 0.75 mm layer of mercury. This cell was irradiated using a 7 ns duration 1.064 μm YAG laser, the mercury layer absorbing the laser beam and acting as an embedded acoustic source of pulses with $<$5 ns duration. LIAD took place from a metal film coated on the outer surface of the cell opposite to the incoming laser beam, and it was observed that large particles (20 μm of Al_2O_3) placed on this surface were ejected by the reflected acoustic pulse. When used as the source in a time-of-flight mass spectrometer, it was found that low mass ion signals were generated by LIAD from a bare gold surface and from a hydrogen-saturated palladium layer. When coated with a MALDI matrix containing a protein (e.g., picolinic acid with insulin or cytochrome analyte), molecular ion signals of the matrix and intact protein were detected. A comparison with direct MALDI desorption from the surface showed that the ion peak delay times were consistent with an acoustic wave having propagated from the mercury layer to the cell surface. Although these experiments appear to provide unequivocal evidence for acoustically induced desorption, the precise mechanism involved remains uncertain for, as noted above, it seems unlikely that molecular size species can be directly desorbed in the same way. The authors do not report postexposure microscopic examination of the surface of their targets, so it is not known whether micromechanical fracture of the MALDI matrix occurred in these experiments.

Vertes and Gijbels[122] have discussed the possible role of thermally induced stress in the MALDI process. Modeling[126] of the interaction (e.g., for a CO_2 laser irradiated alkali halide) has shown that a large stress pulse can be generated prior to the system undergoing a significant temperature rise. Under these conditions molecules could be released through "mechanical fragmentation" without thermal decomposition taking place. Zenobi and Knochenmuss critically appraise these stress-related mechanisms in their comprehensive review of MALDI ion formation.[123]

Very often solid MALDI samples that yield the best ion signals are prepared from solutions that crystallize to form heterogeneous substrates, for example, consisting of a myriad of microscopic crystals. The laser interaction from the thermomechanical perspective is then considerably more complicated than for a homogeneous surface. As the microcrystals can present accessible rear surfaces the possibility cannot be ruled out that stress transients generated by

vaporization from their front surface lead to desorption through mechanical unloading wave effects akin to those described by Lidner and Seydel[127] and Golovlev et al.[124] It is also conceivable that microcrystals in the form of cylinders might be fragmented by internal focusing of tensile stress waves in a fashion similar to that seen in soft materials.[41]

There have been few studies of acoustic transients generated in conventional front-surface irradiated MALDI so that experimental evidence to support stress wave effects in desorption is lacking. One exception is the work of Taranenko et al.,[128] who applied fast piezoelectric transducers to monitor the absorption of 266 and 355 nm laser radiation in MALDI matrices through the thermoelastic stress waves generated by rapid heating. A nonlinear scaling of acoustic signal amplitude with fluence was observed for some wavelength−sample combinations and attributed to multistep absorption rather than ablation recoil. Unfortunately, the authors do not report quantified measurements of the stress wave amplitude of the thermoelastic stress waves, so it remains speculation as to whether photomechanical effects are contributory in MALDI. Given that UV optical penetration depths in samples are small (typically ~50 nm, $\mu_a \sim 2 \times 10^7$ m^{-1}) and that the laser pulse duration is usually greater than a nanosecond, stress relaxation is rapid, resulting in a large attenuation factor A_{ac} (eq 12). For example, with parameters appropriate to UV MALDI, we can estimate that τ will be >40 and the corresponding attenuation factor $A_{ac} \leq 0.025$. Even so, the predicted peak thermoelastic stress generated in typical MALDI experiments can be quite large, with rough estimates based on eqs 3 and 12 giving ~10^6−10^7 Pa. If the laser pulse is quasi-symmetric, compressive and tensile stress components of this magnitude will be generated and propagate in the sample.

In the IR laser interaction lower values of μ_a are encountered for matrices and the more extensive thermomechanical effects may lead to spallation. Cramer et al.[129] have discussed this possibility with regard to ion formation in IR MALDI using a free-electron laser (FEL) source. The output of this FEL was in the form of variable duration macropulses composed of a train of 1−2 ps micropulses and was tuneable over the 2.65−6.5 μm wavelength range. In the experiments it was found that desorbed ions appeared at much lower energy density loadings in the matrix than for UV MALDI and that for pulses >100 ns, irradiance rather than fluence was the characterizing parameter. To explain this behavior spallation-induced fracture and associated bond breaking were proposed as one of the possible mechanisms responsible for ion generation. On the basis of the macropulse duration of the FEL they estimated peak stress amplitudes of 50 bar (5×10^6 Pa) would be generated, which might be sufficient to cause spallation fracture of a brittle matrix such as succinic acid. In other related work Belov et al.[130] have studied the CO_2 laser ablation of organic molecules from frozen matrices containing tyrosine and tryptophan as analytes. Resonance-enhanced multiphoton ionization of molecules in the plume was used to produce molecular ions that could be detected by mass spectrometry. In the experiments they noted a faint blue emission from the frozen aqueous ethanol matrix which, by analogy with results for liquid ablation, they attributed to sonoluminescence. It was postulated that this emission was induced by collapsing cavitation bubbles generated by a pressure wave in the liquid, although they do not quantify this theory. Strong heating of vaporized gas by the bubble collapse was used to explain the onset of molecular fragmentation that was observed at a fluence ~1.2 times greater than the ablation threshold of 1.7×10^4 J m^{-2}.[130]

The recent molecular dynamic (MD) simulations reported by Zhigilei and Garrison[60] offer interesting insight into the potential role of photomechanical effects in the ablation of MALDI-type organic materials. As discussed earlier, the MD simulations predict significant differences in the ablation mechanisms for the thermal and stress confinement regimes. In the former, phase explosions play a major role, expelling material as a coexisting mixture of vapor, clusters, and droplets, a concept previously invoked to explain the stoichiometric laser ablation of complex compounds,[131] as well as the dynamics of laser-ablated metals.[113] When the laser pulse is sufficiently short that there is stress confinement, the tensile stress generated by expansion of the free surface leads to photomechanical rupture on the front surface of the substrate. We note that these MD simulations were performed for 15 and 150 ps duration pulses, which are short compared to most typical MALDI experiments, where lasers commonly have durations of a few nanoseconds or longer. With nanosecond pulses there is thermal confinement but not stress confinement so, as noted earlier, the magnitude of stress transients will be greatly attenuated. The application of MD simulations to determine stress generation in this longer pulse regime would be useful, particularly as the complex sample microstructure and transient nature of the interaction make it difficult to probe the mesoscopic scale of the MALDI interaction experimentally.

VIII. Laser-Induced Surface Cracking

The formation of microcracks on the surface of crystalline materials and amorphous glasses as a result of laser exposure in or near the ablation regime is of interest from a number of viewpoints. In laser ablation−deposition quite large solid fragments may be ejected from the surface, compromising the integrity of a deposited film as well as altering the target surface and possibly its ablation properties.[132] The deliberate microcrazing of glass surfaces has applications in laser marking, as the irradiated regions stand out in better contrast to the unexposed surface, rendering the marks more legible.[133] However, if fragments become detached in large quantities, this may be problematic, as there is a need to filter and remove potentially hazardous particulate debris in an industrial marking situation. In laser micromachining of glass microcomponents it is usually vital to avoid cracking completely, as this produces undesirable surface quality and may weaken the compo-

nent through incipient crack formation sites.

The explanation of surface microcracking in laser-irradiated glass and other materials has often simply been put down to the large thermal stress induced in the laser heating phase of the interaction.[134,135] This appears to overlook the fact that brittle materials can be very strong in compression, and it is much more likely that tensile stress accompanying the interaction is responsible for failure. Two photomechanical stress sources may play a role in initiating cracking—that generated by transient tensile stress components produced in the heating phase and that originating from thermoelastic stress in the cooling phase of the interaction.

The first of these follows from the fact that a longitudinal stress wave propagating normal to the surface will also generate a lateral (in-plane) stress component, the magnitude of which can be estimated from eq 3 for an isotropic solid. For laser spot sizes that are large compared to μ_a^{-1} so that the acoustic source is one-dimensional, the in-plane strain is zero and outside the laser-heated zone where $\Delta T = 0$

$$\sigma_{22} = \nu\sigma_{11}/(1 - \nu) \tag{40}$$

where σ_{11} is the stress normal to the surface and σ_{22} ($= \sigma_{33}$) is the in-plane stress component. Thus, the tensile component of the bipolar longitudinal stress wave is accompanied by a transient in-plane tension, which could play a role in initiating through-plane cracks that can penetrate to the surface. Dickinson and co-workers[132,136] have reported very comprehensive studies of the interaction of the 248 nm KrF laser with wide band-gap single crystals (e.g., MgO and NaCl) and concluded that mechanical deformation plays a major role in the ablation process. For these materials the band gap is much larger than the laser photon energy and absorption occurs as a result of defects in the crystal lattice. For high fluence irradiation repeated exposure of the surface produces cyclic thermal stress, mechanical deformation, and fracture. This acts to build up additional defects in the lattice, which increase the target absorptivity and ultimately result in a sufficiently high surface temperature being reached that there is a transition to thermally induced ablation. A feature of the irradiation site is the appearance of very regular cracks forming along cleavage planes. Depending on the crystal orientation minute rectangular or triangular fragments of the crystal become completely detached in this process.[132] Similar microcracking is seen on the surface of 248 nm laser irradiated $SrTiO_3$ single crystals[137] and, at high fluence, in various fluoride crystals.[138] In the latter case the authors note a high density of short cracks appearing at the periphery of the irradiation site, where there is a large local shear stress. Three-dimensional solutions of the quasi-static thermoelastic stress equation support this view.[24,25] This behavior is not exclusive to UV exposure as it has also been observed in MgO crystals irradiated with a pulsed 10.6 μm CO_2 laser, supporting the concept that thermal stress is involved in the surface microcracking.[139]

In glasses exposed to pulsed lasers the main contribution to surface failure and cracking appears to be tensile thermoelastic stress. Although, in the initial stage of heating, the glass temperature rise can produce substantial compressive stress, this cannot reach a sufficient magnitude to initiate failure by compression before the glass viscosity drops to a low value. Then, being "liquidlike", with a $\sigma_{11} = 0$ boundary condition, $\sigma_{11} \sim \sigma_{22} \sim \sigma_{33} \sim 0$ and the melt is in a low state of stress. In the cooling phase, when heat diffuses into the bulk glass, the temperature fall can be fast enough for "strain-freezing" to occur; that is, the glass becomes a very high viscosity solid well before it cools to the ambient temperature. If strain-freezing occurs at a temperature ΔT_m above ambient, modeling shows that the residual thermoelastic stress is tensile with a magnitude[133]

$$\sigma_{22} = \sigma_{33} = \frac{E\alpha\Delta T_m}{1 - \nu} = \frac{B\beta(1 - 2\nu)\Delta T_m}{1 - \nu} \tag{41}$$

where α is the linear thermal expansivity and E is Young's modulus. For soda lime glass irradiated with a pulsed CO_2 laser ($\mu_a \approx 10^5$ m^{-1}), strain-freezing occurs at $\Delta T_m \approx 750$ K, producing in-plane stress levels of 6×10^8 Pa, which is well above that for tensile failure of the glass. Microcracks extending over the full irradiated area are produced above a threshold fluence ($\sim 1.5 \times 10^4$ J m^{-2}) and in some cases entire platelets fracture from the surface. Supporting evidence for this model comes from the observation that surface cracking may be delayed to long after laser exposure, suggesting the glass has been place in a metastable state of tensile stress, and also from deflection measurements of thin irradiated plates, which confirm the surface is in tension.[133] As would be expected, the properties of the glass are important in determining whether there is microcrazing, that is, through the appearance of α and ΔT_m in eq 41. The depth of the strain-frozen layer is also a determining factor in cracking, as energetic considerations show it can influence the size of through-cracks that can grow laterally. This may explain why UV lasers that are strongly absorbed in a glass, and produce a more shallow heat-affected zone, have a lower propensity for causing microcracking.[134,135]

A residual normal surface strain is predicted to accompany strain-freezing, with a value that follows from the analysis of Allcock et al.[133]

$$\epsilon_{11} = 2\alpha\nu\Delta T_m/(1 - \nu) \tag{42}$$

Due to this strain, in the absence of any ablative removal, the final surface height will be above its initial level. For soda lime glass with $\Delta T_m = 750$ K, the size of this "bump" found using eq 42, is $\epsilon_{11}\mu_a^{-1} \approx 37$ nm if irradiation is with the CO_2 laser ($\mu_a^{-1} \approx 10$ μm) and there is heat confinement. Shiu et al.,[140] using atomic force microscopy, have observed and quantified these "bumps" in glasses exposed over a spot radius of ~ 31 μm by a microsecond duration CO_2 laser. Depending on the glass type, they measured bump heights in the $\sim 10-100$ nm range and noted that the surface will develop in-plane tensile stress, although they do not report any cracking. Their explanation of the underlying mechanism is similar

to that of Allcock et al.'s[133] but leads to somewhat different expression for the free-strain as it based on differential expansion between the liquid and solid phases of the glass. It should be noted that the aspect ratio of the spot radius to heated depth is quite small in their work, so that the simplifying assumptions of one-dimensional thermoelastic stress and heat flow embodied in eqs 41 and 42 will not strictly be applicable. The stress field is then more complicated because of boundary effects.[25]

IX. Photomechanical Effects in Laser Cleaning

Laser cleaning is applicable in a diverse range of areas, but of particular interest from the aspect of photomechanical ablation is its use for removing micrometer and sub-micrometer particles from semiconductor wafers and data-storage devices. The various approaches to laser cleaning for the removal of surface particulates (e.g., of metals and organic residues) have been reviewed by Tam et al.[141] These can be classified as "dry cleaning" and "steam cleaning", according to whether the as-received surface is directly treated or a liquid layer/film is deliberately added to aid ablative removal.

In one form of dry cleaning, a laser wavelength is chosen that is strongly absorbed by the substrate that is contaminated with particles.[141] Under short pulse laser exposure the substrate heats rapidly, generating stress transients and corresponding particle displacements as the surface adjusts to its new thermal equilibrium position. Although the magnitude of surface displacement produced by the thermal expansion is small, a very large acceleration and then deceleration are produced if the laser heating pulse is in the sub-microsecond range. The effect of this mechanical motion is to produce an inertial force on surface particles causing their ejection (ablation) if the physical forces (e.g., van der Waals and capillary force) that bind them to the surface are overcome.

The precise mechanisms involved in the dry cleaning interaction are, in general, complicated and depend on whether the particles are optically transparent on a laser absorbing substrate, absorbing on a transparent substrate or a combination of both applies. A useful gauge of the magnitude of the effect can be gained, however, by estimating the surface acceleration forces on particles. If there is no stress confinement ($t_p/t_{ac} \gg 1$), determination of the acceleration is straightforward as the surface adjusts essentially instantaneously to the new thermal equilibrium position. The surface displacement is then

$$u(t) = \alpha(1 + \nu)\langle \Delta T(t)\rangle \, \mathrm{d}(t)/(1 - \nu) \qquad (43)$$

where $\mathrm{d}(t)$ is the depth into the surface over which there is a mean temperature rise $\langle \Delta T(t)\rangle$. For thermal confinement $\mathrm{d}(t) = \mu_a^{-1}$ is constant, whereas when heat diffusion dominates $\mathrm{d}(t) \sim (Dt)^{1/2}$, where D is the thermal diffusivity. Using

$$\langle \Delta T(t)\rangle \, \mathrm{d}(t) = \frac{1}{\rho C}\int_0^t E_0(t')\, \mathrm{d}t' \qquad (44)$$

where E_0 is the laser irradiance, the surface velocity becomes

$$\frac{\mathrm{d}u}{\mathrm{d}t} = \frac{\alpha(1 + \nu)E_0(t)}{(1 - \nu)\rho C} \qquad (45)$$

and is proportional to $E_0(t)$. The surface acceleration is given by

$$a = \frac{\mathrm{d}^2u}{\mathrm{d}t^2} = \frac{\alpha(1 + \nu)\ \mathrm{d}E_0(t)}{(1 - \nu)\ \rho C\quad \mathrm{d}t} \qquad (46)$$

where $\mathrm{d}E_0/\mathrm{d}t$ is now the rate of change of irradiance. For a silicon substrate with $\nu = 0.28$ for the [100] plane, $\alpha = 2.2 \times 10^{-6}$ K^{-1}, a laser pulse of peak irradiance 10^{11} W m^{-2} and $t_p = 10$ ns, it is found from eq 43 that $u = 1.4$ nm at the end of the pulse. In this example the heated depth at 10 ns would be $\sim$0.89 μm, assuming that thermal diffusion dominates for a strongly absorbing substrate [i.e., $\mu_a^{-1} \ll (Dt_p)^{1/2}$]. Although only a very small displacement is produced, if the laser pulse has a 5 ns rise time and 5 ns fall time, the acceleration/deceleration found from eq 46 reaches $\pm$ 2.8 $\times$ 10^7 m s^{-2} due to the very short heating time. If a particle of radius r and mass M on the surface is assumed to be nonperturbing (i.e., transparent and with a radius satisfying $r < \mathrm{d}\rho_S/\rho$, where ρ_S and ρ are the substrate and particle mass densities, respectively), then this deceleration will exert on it an inertial force of $F \sim Ma$. For example, this will be approximately valid for a particle of radius r =200 nm and mass $M = 7.8 \times 10^{-17}$ kg ($\rho_S = \rho = 2330$ kg m^{-3}). In this case the force is $F = 2.2 \times 10^{-9}$ N, and there would be a corresponding impulsive kinetic energy transfer to the particle of $M(\mathrm{d}u/\mathrm{d}t)^2/2 \approx 5$ eV.

Tam et al.[141] report that with 20 ns KrF laser pulses, this direct photomechanical ablation mechanism is effective in removing most types of micrometer-scale particles from various surfaces. They note, however, that the efficiency is enhanced if a thin liquid film is added to the surface so as to aid removal by explosive superheating. Measurements of the acceleration of a silicon surface irradiated with a 532 nm wavelength Q-switched YAG laser producing 10 and 20 ns duration pulses have been made using a heterodyne interferometer.[142] The findings confirm that accelerations are in keeping with the predictions of the simple modeling, with $a \approx 10^7$ m s^{-2} being recorded at a fluence of 800 J m^{-2} ($E_0 \sim 8 \times 10^{10}$ W m^{-2}). More refined laser dry cleaning models have recently been developed by Luk'yanchuk et al., which account for the thermal contact of particles with the substrate and the optical enhancement effects produced by the particle itself.[143] In the laser cleaning of polymers, also particle expansion has been identified as a cleaning mechanism.[144]

The force and energy requirements for the removal of small particles on surfaces have been analyzed by Kolomenskii et al.[145] In this paper they also describe an alternative approach to the photomechanical ablation of particles that uses 10 ns duration 337 nm nitrogen or 1.06 μm Nd:YAG laser pulses focused on a silicon substrate to drive surface acoustic waves (SAWs).[145] As the Rayleigh-type SAWs propagate out from the source, they produce large accelerations/decelerations normal to the surface, causing particle

removal over a wide area and not solely at the laser spot. When the YAG laser was used at high irradiance so as to produce breakdown at the silicon surface, the SAW amplitude and acceleration were very large, with experimental values as high as $\sim 1.9 \times 10^9$ ms^{-2} being recorded.[145] This enables removal of sub-micrometer particles. They also present results of modeling the normal velocity and acceleration of the SAWs in the linear and nonlinear propagation regimes. The authors predict that constraints set by surface fracture and SAW attenuation will limit the smallest radius of particles that can be removed from silicon in this way to ~25 nm.

X. Summary and Conclusions

In this review we have outlined the basic physical principles that give rise to transient pressure waves in liquids as well as transient and quasi-static stresses in solid materials under pulsed laser irradiation. Transient mechanical effects arise when a solid or a liquid is heated with a laser pulse shorter than or comparable with the finite time the irradiated volume needs to thermally expand to its new equilibrium size. Additionally, for solids, quasi-static thermoelastic stresses can develop because of the presence of boundary constraints that prevent expansion; these may persist over quite long time scales, that is, similar to the thermal relaxation time. Both compressive and tensile forces are generated in this way, but for photomechanical ablation it is the tensile stress that is usually of most interest because materials tend to fail more readily under tension than compression.

There have been a number of reports of low threshold ablation that require for their explanation that photomechanical as opposed to photothermal vaporization is the main driving force for material removal. The energetic efficiency advantage of a photomechanical fragmentation versus a photothermal vaporization mechanism is huge, but the fraction of optical energy that goes into mechanical energy and is available for the fragmentation process is, on the other hand, very small. From the body of published work on liquids there seems little doubt that a photomechanical mechanism can play a major role in initiating low threshold ablation. For biological tissue and solids the evidence is less clear and there appear to be significant discrepancies among the findings of different researchers. Considerable care is needed when interpreting an unknown ablation process as initiated by photomechanical effects, and simple qualitative arguments concerning stress generation alone can be insufficient to reach a sound conclusion. Knowledge of factors such as the magnitude and time history of the stress and the material properties at temperatures up to and including that at which ablation is initiated as well as the energetic requirements for mechanical photofragmentation is also necessary. There is still considerable scope for further research aimed at gaining improved understanding of the interaction, for example, making use of model systems for which the main influencing factors can be clearly specified and controlled. For soft media such as biological tissue this research has important practical implications to optimize laser exposures to achieve material removal with minimal collateral thermal damage.

An awareness and understanding of stress-related effects is also relevant for a number of other systems of practical importance. These include, for example, layered structures where the release of stored thermoelastic energy has been proposed as the driving force for low-threshold film ejection. In MALDI analysis there is a growing belief that mechanical effects may under certain instances be contributory to intact molecular ion release, although the exact physical mechanisms involved (fracture mediated, direct "mechanical" desorption?) remain unclear. Finally, photomechanical effects can be exploited for removal of microscopic particles from surfaces with applications in laser cleaning of technologically important substrates and components.

We conclude by noting that when photomechanical effects contribute to material removal in short pulse laser interactions they will, in most circumstances, likely do so in concert with other ablation mechanisms. Thus, determining the role of photomechanical effects is a difficult problem, but one that offers an exciting challenge for both experimental and theoretical researchers.

XI. References

(1) Steverding, B. *J. Phys. D* **1971**, *4*, 787.
(2) Dingus, R. S.; Scammon, R. J. *Proc. SPIE* **1991**, *1427*, 45.
(3) Dingus, R. S.; Curran, D. R.; Oraevsky, A. A.; Jacques, S. L. *Proc. SPIE* **1994**, *2134A*, 434.
(4) Dingus, R. S.; Scammon, R. J. *Springer Lect. Notes Phys.* **1991**, *389*, 180.
(5) Albagli, D.; Perelman, L.; Janes, G.; von Rosenberg, C.; Itzkan, I.; Feld, M. *Lasers Life Sci.* **1994**, *6*, 55.
(6) Carome, E. F.; Clark, N. A.; Moeller, C. E. *Appl. Phys. Lett.* **1964**, *4*, 95.
(7) Venugopalan, V.; Nishioka, N. S.; Mikic, B. B. *Biophys. J.* **1996**, *70*, 2981.
(8) Tolbert, W. A.; Lee, I.-Y. S.; Doxtader, M. M.; Ellis, E. W.; Dlott, D. D. *J. Imaging Sci. Technol.* **1993**, *37*, 411.
(9) Adrian, F. J.; Bohandy, J.; Kim, B. F.; Jette, A. N.; Thompson, P. *J. Vac. Sci. Technol. B* **1987**, *5*, 1490.
(10) Fukumura, H.; Kohji, Y.; Nagasawa, K.; Masuhara, H. *J. Am. Chem. Soc.* **1994**, *116*, 10304.
(11) Doukas, A. G.; Flotte, T. J. *Ultrasound Med. Biol.* **1996**, *22*, 151.
(12) Watanabe, S.; Flotte, T. J.; McAuliffe, D. J.; Jacques, S. L. *J. Invest. Dermatol.* **1988**, *90*, 761.
(13) Grady, D. E. *J. Mech. Phys. Solids* **1988**, *36*, 353.
(14) Eliezer, S.; Gilath, I.; Bar-Noy, T. *J. Appl. Phys.* **1990**, *67*, 715.
(15) Zel'dovich, Y. B.; Raizer, Y. P. *Physics of Shock Waves and High-Temperature Hydrodynamic Phenomena*; Academic Press: London, U.K., 1967; Vol. II.
(16) Jacques, S. L. *Surg. Clin. North Am.* **1992**, *72*, 531.
(17) Oraevsky, A. A.; Esenaliev, R.; Letokhov, V. S. In *Laser Ablation, Mechanisms and Applications*; Springer: New York, 1991; p 112.
(18) van Leeuwen, T. G.; Jansen, E. D.; Motamedi, M.; Borst, C.; Welch, A. J. In *Optical-Thermal Response of Laser-Irradiated Tissue*; Plenum Press: New York, 1995; p 709.
(19) Dyer, P. E.; Srinivasan, R. *Appl. Phys. Lett.* **1986**, *48*, 445.
(20) Gusev, V. E.; Karabutov, A. A. *Laser Optoacoustics*; American Institute of Physics: New York, 1993.
(21) Vogel, A. *Optical Breakdown in Water and Ocular Media, and Its Use for Intraocular Photodisruption*; Shaker: Aachen, Germany, 2001.
(22) Royer, D.; Dieulesaint, E. *Elastic Waves in Solids I, II*; Springer: Berlin, 2000.
(23) Itzkan, I.; Albagli, D.; Dark, M.; Perelman, L.; von Rosenberg, C.; Feld, M. S. *Proc. Natl. Acad. Sci. U.S.A.* **1995**, *92*, 1960.
(24) Albagli, D.; Dark, M.; von Rosenberg, C.; Perelman, L.; Itzkan, I.; Feld, M. *Med. Phys.* **1994**, *21*, 1323.
(25) Albagli, D.; Dark, M.; Perelman, L. T.; von Rosenberg, C.; Itzkan, I.; Feld, M. S. *Opt. Lett.* **1994**, *19*, 1684.
(26) Koulikov, S. G.; Dlott, D. D. *J. Photochem. Photobiol.* **2001**, *145*, 183.
(27) Bushnell, J. C.; McCloskey, D. J. *J. Appl. Phys.* **1968**, *39*, 5541.

(28) Paltauf, G.; Schmidt-Kloiber, H. *Appl. Phys. A* **1996**, *62*, 303.
(29) Lamb, D. C.; Doukas, A.; Flotte, T. J.; Ossoff, R. H.; Reinisch, L.; Tribble, J. *Proc. SPIE* **1995**, *2391*, 192.
(30) Oraevsky, A. A.; Jacques, S. L.; Tittel, F. K. *Appl. Opt.* **1997**, *36*, 402.
(31) Karabutov, A. A.; Podymova, N. B.; Letokhov, V. S. *Appl. Phys. B* **1996**, *63*, 545.
(32) Paltauf, G.; Schmidt-Kloiber, H. *J. Appl. Phys.* **2000**, *88*, 1624.
(33) Sigrist, M. W. *J. Appl. Phys.* **1986**, *60*, R83−R121.
(34) Landau, L. D.; Lifschitz, E. M. *Hydrodynamik*; Akademie: Berlin, Germany, 1981.
(35) Khan, M. I.; Sun, T.; Diebold, G. J. *J. Acoust. Soc. Am.* **1993**, *94*, 931.
(36) Paltauf, G.; Schmidt-Kloiber, H.; Frenz, M. *J. Acoust. Soc. Am.* **1998**, *104*, 890.
(37) Frenz, M.; Paltauf, G.; Schmidt-Kloiber, H. *Phys. Rev. Lett.* **1996**, *76*, 3546.
(38) Diebold, G. J.; Sun, T. *Acustica* **1994**, *80*, 339.
(39) Jacques, S. L.; Oraevsky, A. A.; Thompson, R.; Gerstman, B. S. *Proc. SPIE* **1994**, *2134A*, 54.
(40) Sun, J. M.; Gerstman, B. S. *Phys. Rev. E* **1999**, *59*, 5772.
(41) Paltauf, G.; Schmidt-Kloiber, H. *Appl. Phys. A* **1999**, *68*, 525.
(42) Zhigilei, L. V.; Garrison, B. J. *Appl. Surf. Sci.* **1998**, *127*−*129*, 142.
(43) Dark, M. L.; Perelman, L. T.; Itzkan, I.; Schaffer, J. L.; Field, M. S. *Phys. Med. Biol.* **2000**, *45*, 529.
(44) Gilath, I.; Eliezer, S.; Dariel, M. P.; Kornblit, L. *Appl. Phys. Lett.* **1988**, *52*, 1207.
(45) Johnson, J. N. *J. Appl. Phys.* **1981**, *52*, 2812.
(46) Seaman, L.; Curran, D. R.; Shockey, D. A. *J. Appl. Phys.* **1976**, *47*, 4814.
(47) Tuler, F. R.; Butcher, B. M. *Int. J. Fracture Mech.* **1968**, *4*, 431.
(48) Fortov, V. E.; Kostin, V. V.; Eliezer, S. *J. Appl. Phys.* **1991**, *70*, 4524.
(49) Kwak, H.-Y.; Panton, R. L. *J. Phys. D: Appl. Phys.* **1985**, *18*, 647.
(50) Fisher, J. C. *J. Appl. Phys.* **1948**, *19*, 1062.
(51) Young, F. R. *Cavitation*; McGraw-Hill: London, U.K., 1989.
(52) Wentzell, R. A.; Lastman, G. J. In *Cavitation and Inhomogeneities*; Springer: Berlin, Germany, 1980; p 72.
(53) Wentzell, R. A.; Lastman, G. J. *Phys. Fluids* **1983**, *26*, 638.
(54) Strauss, M.; Kaufman, Y.; Sapir, M.; Amendt, P.; London, R. A.; Glinsky, M. E. *Proc. SPIE* **1999**, *3601*, 178.
(55) Strauss, M.; Kaufman, Y.; Sapir, M.; Amendt, P.; London, R. A.; Glinsky, M. E. *J. Appl. Phys.* **2002**, *91*, 4720.
(56) Cole, R. H. *Underwater Explosions*; Dover: New York, 1948.
(57) Oraevsky, A. A.; Jacques, S. L.; Tittel, F. K. *J. Appl. Phys.* **1995**, *78*, 1281.
(58) Glinsky, M. E.; Bailey, D. S.; London, R. A. *Proc. SPIE* **1997**, *2975*, 374.
(59) Antoun, T.; Seaman, L.; Glinsky, M. E. *Proc. SPIE* **1995**, *2391*, 413.
(60) Zhigilei, L. V.; Garrison, B. J. *J. Appl. Phys.* **2000**, *88*, 1281.
(61) Oraevsky, A. A.; Jacques, S. L.; Esenaliev, R.; Tittel, F. K. *Lasers Surg. Med.* **1996**, *18*, 231.
(62) Oraevsky, A. A.; Esenaliev, R.; Jacques, S. L.; Tittel, F. K. *Proc. SPIE* **1995**, *2391*, 300.
(63) Kim, D.; Ye, M.; Grigoropoulos, C. P. *Appl. Phys. A* **1998**, *67*, 169.
(64) Paltauf, G.; Reichel, E.; Schmidt-Kloiber, H. *Proc. SPIE* **1992**, *1646*, 343.
(65) Paltauf, G.; Schmidt-Kloiber, H. *Lasers Surg. Med.* **1995**, *16*, 277.
(66) Esenaliev, R.; Jacques, S. L. *Proc. SPIE* **1996**, *2681*, 185.
(67) Oraevsky, A. A.; Esenaliev, R.; Jacques, S. L.; Tittel, F. K. *Proc. SPIE* **1995**, *2323*, 250.
(68) Albagli, D.; Banish, B.; Dark, M.; Janes, G.; von Rosenberg, C.; Perelman, L.; Itzkan, I.; Feld, M. S. *Lasers Surg. Med.* **1994**, *14*, 374.
(69) Paltauf, G.; Schmidt-Kloiber, H. *J. Appl. Phys.* **1997**, *82*, 1525.
(70) Zweig, A. D.; Venugopalan, V.; Deutsch, T. F. *J. Appl. Phys.* **1993**, *74*, 4181.
(71) Venugopalan, V.; Nishioka, N. S.; Mikic, B. B. *Biophys. J.* **1995**, *69*, 1259.
(72) Srinivasan, R.; Braren, B.; Dyer, P. E. *Lasers Surg. Med.* **1987**, *6*, 514.
(73) Dyer, P. E.; Al-Dhahir, R. K. *Proc. SPIE* **1990**, *1202*, 46.
(74) Ghosh, A. P.; Hurst, J. E. *J. Appl. Phys.* **1988**, *64*, 287.
(75) Esenaliev, R.; Oraevsky, A. A.; Letokhov, V. S.; Karabutov, A. A.; Malinsky, T. V. *Lasers Surg. Med.* **1993**, *13*, 470.
(76) Esenaliev, R.; Oraevsky, A. A.; Jacques, S. L.; Tittel, F. K. *Proc. SPIE* **1996**, *2681*, 326.
(77) Tsuboi, Y.; Fukumura, H.; Masuhara, H. *J. Phys. Chem.* **1995**, *99*, 10305.
(78) Golovlyov, V. V.; Letokhov, V. S. *Appl. Phys. B* **1993**, *57*, 417.
(79) Tsuboi, Y.; Hatanaka, K.; Fukumura, H.; Masuhara, H. *J. Phys. Chem.* **1994**, *44*, 11237.
(80) Kim, D.; Grigoropoulos, C. P. *Appl. Surf. Sci.* **1998**, *127*−*129*, 53.
(81) Niemz, M. H.; Klancnik, E. G.; Bille, J. F. *Lasers Surg. Med.* **1991**, *11*, 426.
(82) Vogel, A. *Phys. Med. Biol.* **1997**, *42*, 895.
(83) Vogel, A.; Noack, J.; Huettmann, G.; Paltauf, G. *Proc. SPIE* **2002**, *4633*, 23.
(84) Duck, F. A. *Physical Properties of Tissue*; Academic Press: London, U.K., 1990.
(85) Dombi G. W.; Haut R. C.; Sullivan W. G. *J. Surg. Res.* **1993**, *54*, 21.
(86) Haut R. C. *Trans. ASME Biomed. Eng.* **1989**, *111*, 136.
(87) Vogel, H. G. *Biochim. Biophys. Acta* **1972**, *286*, 79.
(88) Majaron, B.; Plestenjak, P.; Lukac, M. *Appl. Phys. B.* **1999**, *69*, 71.
(89) Venugopalan, V. *Proc. SPIE* **1995**, *2391*, 300.
(90) Hoffman, H. J.; Telfair, W. B. *J. Refractive Surg.* **2000**, *16*, 90.
(91) Telfair, W. B.; Bekker, C. H. H. J.; Yoder, P. R.; Nurdquist, R. E.; Eiferman, R. A.; Zenzie, H. H. *J. Refractive Surg.* **2000**, *16*, 40.
(92) Hoffman, H. J.; Telfair, W. B. *J. Biomed. Opt.* **1999**, *4*, 465.
(93) Shori, R. K.; Walston, A. A.; Stafsudd, O. M.; Fried, D.; Walsh, J. T. *IEEE J. Selected Topics Quantum Electron.* **2001**, *7*, 959.
(94) Bäuerle, D. *Laser Processing and Chemistry*; Springer: Heidelberg, Germany, 2000.
(95) Gower, M. C. In *Laser Processing in Manufacturing*; Chapman and Hall: London, U.K., 1993.
(96) Chrisey, D. B.; Hubler, G. K. *Pulsed Laser Deposition of Thin Films*; Wiley-Interscience: New York, 1994.
(97) Hare, D. E.; Franken, J.; Dlott, D. D. *J. Appl. Phys.* **1995**, *77*, 5950.
(98) Dyer, P. E. In *Photoacoustic and Photothermal Phenomena*; Springer: Heidelberg, Germany, 1988; p 164.
(99) Costela, A.; Figuera, J. M.; Florido, F.; Garciamoreno, I.; Collar, E. P.; Sastre, R. *Appl. Phys. A* **1995**, *60*, 261.
(100) Srinivasan, R.; Braren, B.; Sutcliffe, E. *Appl. Phys. Lett.* **1987**, *51*, 1285.
(101) Chuang, T. J.; Hiraoka, H.; Modl, A. *Appl. Phys. A* **1988**, *45*, 277.
(102) Srinivasan, R.; Braren, B. *Appl. Phys. A* **1988**, *45*, 289.
(103) Cross, F. W.; Al-Dhahir, R. K.; Dyer, P. E. *J. Appl. Phys.* **1988**, *64*, 2194.
(104) Cross, F. W.; Al-Dhahir, R. K.; Dyer, P. E.; MacRober, A. J. *Appl. Phys. Lett.* **1987**, *50*, 1019.
(105) Aldhahir, R. K.; Dyer, P. E.; Zhu, Z. *Appl. Phys. B* **1990**, *51*, 81.
(106) Kukreja, L. M.; Hess, P. *Appl. Phys. Lett.* **1993**, *62*, 205.
(107) Dyer, P. E.; Sidhu, J.; Oldershaw, G. A. *Appl. Phys. B* **1989**, *48*, 489.
(108) Dyer, P. E.; Sidhu, J.; Tait, B. L. *IEEE Trans. Ultrason., Ferroelect., Freq. Contr.* **1988**, *35*, 2.
(109) Zweig, A. D.; Deutsch, T. F. *Appl. Phys. B* **1992**, *54*, 76.
(110) Marshall, J.; Krueger, R. R.; Rothery, S.; Trokel, S. *Br. J. Ophthalmol.* **1986**, *70*, 482.
(111) Yashima, Y.; Mcauliffe, D. J.; Flotte, T. J. *Lasers Surg. Med.* **1990**, *10*, 280.
(112) Dyer, P. E.; Farrar, S.; Key, P. H. *Appl. Phys. Lett.* **1992**, *60*, 1890.
(113) Miotello, A.; Kelly, R. *Appl. Phys. Lett.* **1995**, *67*, 3535.
(114) Murray, T. W.; Wagner, J. W. *J. Appl. Phys.* **1999**, *85*, 2031.
(115) Scruby, C. B.; Drain, L. E. *Laser Ultrasonics*; Adam Hilger: Bristol, U.K., 1990.
(116) Dewhurst, R. J.; Hutchins, D. A.; Palmer, S. B.; Scruby, C. B. *J. Appl. Phys.* **1982**, *53*, 4064.
(117) Bresse, L. F.; Hutchins, D. A.; Lundgren, K. *J. Acoust. Soc. Am.* **1988**, *84*, 1751.
(118) Sigrist, M. W.; Nanai, L. *Appl. Phys. Lett.* **1985**, *46*, 256.
(119) Queheillalt, D. T.; Wadley, H. N. G. *J. Appl. Phys.* **1998**, *83*, 4124.
(120) Ablett, S. J.; Dyer, P. E.; Tait, B. L.; Barnes, J. A. *Appl. Phys. Lett.* **1991**, *59*, 3236.
(121) Fukumura, H.; Kohji, Y.; Nagasawa, K.; Masuhara, H. *J. Am. Chem. Soc.* **1994**, *116*, 10304.
(122) Vertes, A.; Gijbels, R. In *Laser Ionization Mass Analysis*; Wiley: New York, 1993; Chapter 3.
(123) Zenobi, R.; Knochenmuss, R. *Mass Spectrom. Rev.* **1998**, *17*, 337.
(124) Golovlev, V. V.; Allman, S. L.; Garrett, W. R.; Taranenko, N. I.; Chen, C. H. *Int. J. Mass Spectrom. Ion Processes* **1997**, *169*−*170*, 69.
(125) Beavis, R. C.; Schlag, E. W.; Lindner, J.; Grotemeyer, J. *Z. Naturforsch. A* **1988**, *43*, 1083.
(126) Vertes, A.; Levine, R. D. *Chem. Phys. Lett.* **1990**, *171*, 284.
(127) Lindner, B.; Seydel, U. *Anal. Chem.* **1985**, *57*, 895.
(128) Taranenko, N. I.; Golovlev, V. V.; Puretzky, A. A.; Allman, S. L.; Chen, C. H. *Chem. Phys. Lett.* **1995**, *234*, 165.
(129) Cramer, R.; Haglund, R. F.; Hillenkamp, F. *Int. J. Mass Spectrom.* **1997**, *169*, 51.
(130) Belov, M. E.; Alimpiev, S. S.; Mlynsky, V. V.; Nikiforov, S. M.; Derrick, P. J. *Rapid Commun. Mass Spectrom.* **1995**, *9*, 1431.
(131) Dyer, P. E.; Farrar, S. R.; Key, P. H. *Appl. Surf. Sci.* **1992**, *54*, 255.

(132) Webb, R. L.; Jensen, L. C.; Langford, S. C.; Dickinson, J. T. *J. Appl. Phys.* **1993**, *74*, 2323.
(133) Allcock, G.; Dyer, P. E.; Elliner, G.; Snelling, H. V. *J. Appl. Phys.* **1995**, *78*, 7295.
(134) Buerhop, C.; Blumenthal, B.; Weissmann, R.; Lutz, N.; Biermann, S. *Appl. Surf. Sci.* **1990**, *46*, 430.
(135) Braren, B.; Srinivasan, R. *J. Vac. Sci. Technol., B* **1988**, *6*, 537.
(136) Webb, R. L.; Jensen, L. C.; Langford, S. C.; Dickinson, J. T. *J. Appl. Phys.* **1993**, *74*, 2338.
(137) Benitez, F.; Sanchez, F.; Trtik, V.; Varela, M.; Bibes, M.; Martinez, B.; Fontcuberta, J. *Appl. Phys. A* **1999**, *69*, S501−S504.
(138) Reichling, M.; Sils, J.; Johansen, H.; Matthias, E. *Appl. Phys. A* **1999**, *69*, S743−S747.
(139) Dirnberger, L.; Dyer, P. E.; Farrar, S.; Key, P. H.; Monk, P. *Appl. Surf. Sci.* **1993**, *69*, 216.
(140) Shiu, T. R.; Grigoropoulos, C. P.; Cahill, D. G.; Greif, R. *J. Appl. Phys.* **1999**, *86*, 1311.
(141) Tam, A. C.; Leung, W. P.; Zapka, W.; Ziemlich, W. *J. Appl. Phys.* **1992**, *71*, 3515.
(142) Dobler, V.; Oltra, R.; Boquillon, J. P.; Mosbacher, M.; Boneberg, J.; Leiderer, P. *Appl. Phys. A* **1999**, *69*, S335−S337.
(143) Luk'yanchuk, B. S.; Zheng, Y. W.; Lu, Y. F. Presented at the International Symposium on Intensive Laser Action and its Applications, St. Petersburg, Russia, 2000.
(144) Fourrier, T.; Schrems, G.; Muhlberger, T.; Heitz, J.; Arnold, N.; Bauerle, D.; Mosbacher, M.; Boneberg, J.; Leiderer, P. *Appl. Phys. A* **2001**, *72*, 1.
(145) Kolomenskii, A. A.; Schuessler, H. A.; Mikhalevich, V. G.; Maznev, A. A. *J. Appl. Phys.* **1998**, *84*, 2404.

CR010436C